Astron. Astrophys. 287, 893–926 (1994)

ASTRONOMY AND ASTROPHYSICS

Nonradial and nonpolytropic astrophysical outflows

III. A criterion for the transition from jets to winds

C. Sauty[1] **and K. Tsinganos**[23]

[1] Observatoire de Paris, D.A.E.C., F-92195 Meudon, France
[2] Department of Physics, University of Crete, GR-71409 Heraklion, Crete, Greece
[3] Research Center of Crete, FORTH, GR-71110 Heraklion, Crete, Greece

Received 22 July 1993 / Accepted 20 September 1993

Abstract. A new class of analytical solutions for rotating MHD outflows from the gravitational potential of a central object is discussed; the outflows are driven by thermal pressure gradients arising from a non polytropic heating, as well as by magnetic rotator forces. The solutions are obtained by a separation of the variables, of the spherical distance R and of the magnetic flux function α in several physical key quantities. Thus, the solutions are magnetic flux self-similar and treat fully the dynamics of the flow from its source to large distances. The topology and asymptotical behaviour of this broad class of solutions is examined in detail. At the Alfvénic and X-type critical points which the transAlfvénic solution crosses, the appropriate criticality conditions are applied. Attention is focused on the streamline shape which is calculated exactly and consistently throughout the outflow and allows us to formulate a criterion that distinguishes between collimated jets and non collimated winds. Thus, two classes of solutions with markedly different asymptotics are found. The *first* corresponds to outflows wherein the streamlines obtain asymptotically a conical shape on the poloidal plane, while the *second* is constituted of collimated jet-type outflows wherein the streamlines obtain asymptotically a cylindrical shape. Furthermore, it is shown that a basic feature of such collimated flows is an oscillatory jet width, without the help of an external confining pressure; an analytical formula is given for the wavelength of these oscillations. Hence, the jet does not need to focalize completely along the polar axis, but through successive contractions and expansions in its width, it naturally relaxes into a cylindrical pattern; it is argued that this is due to a consistent treatment of the current flowing along the axis of the jet. The study is applied to the relevant problem of jets from young stellar objects; this preliminary application suggests that several observational constraints are satisfied if we have a two-component outflow, one originating at the star while the other at the surrounding disc. A simple criterion is given for the transition from a magnetic rotator with collimated jets to a slow magnetic rotator with a noncollimated wind, in terms of the meridional anisotropy in the available energy in the streamlines of the outflow; it essentially amounts to saying that if the magnetic rotator results in a surplus of energy along any nonpolar streamline as compared to the available energy along the polar streamline, then the flow collimates into a jet. It is suggested therefore that the shape of the streamlines of the outflow from a rotating object switches over from cylindrical to conical asymptotics, as the central object looses angular momentum and passes successively from the stage of a pre-main sequence YSO to that of a main sequence star.

Key words: MHD – solar wind – ISM: jets and outflows – stars: mass-loss – stars: pre-main sequence – galaxies: jets

1. Introduction

In the last three decades observations have revealed that there exist two wide classes of astrophysical large scale outflows originating from stars and stellar systems. *First*, there is the class of astrophysical *winds* wherein the outflow at large distances from its origin and of the central object obtains radial asymptotics; its prototype is the solar wind which was predicted by Parker's fundamental hydrodynamic theory (1958, 1963) and was later verified by *in situ* measurements at the interplanetary space on the ecliptic plane; imminent measurements from the satellite *Ulysses* outside the ecliptic plane and in the solar polar directions are expected to reveal unmeasured so far wind properties at those large heliographic latitudes.

And *second*, there is the class of astrophysical *jets*, wherein the outflow is collimated at various degrees over long distances along some preferential direction. These supersonic beams were proposed to exist in radio sources as a means of transporting energy from the intense central cores of active galaxies and quasars to their distant lobes (Rees 1971); in recent years the existence of such energy bridges has been also confirmed observationally in many extragalactic objects (Hughes 1991). In particular, in the

Send offprint requests to: C. Sauty

images of the well observed and classical jet in the elliptic galaxy M87 obtained with the VLA as well as with the Faint Object Camera aboard the Hubble telescope (Owen et al 1989; Macchetto 1992), the magnetic vectors suggest that there is present a rather strong toroidal component of the magnetic field; that this jet is indeed highly twisted is also inferred from the fact that the synchrotron emitting regions in the boundary layer of the jet have a much larger pressure than the external medium and therefore confinement could be assisted by magnetic tension. In our Milky Way, similar high-speed bipolar outflows and optical jets have been systematically observed to be associated with star forming systems where accretion disks are also inferred to exist (Lada 1985; Mundt 1985).

From the theoretical point of view three groups of studies have been aimed towards describing the dynamics of a magnetized astrophysical outflow from a rotating gravitating central object. First, the role of the magnetic field in carrying angular momentum and thus braking the rotation of a star (Schatzman 1962; Mestel 1968; Mestel & Spruit 1987), was originally addressed in the approximation of the equatorial plane and for a polytropic gas (Weber & Davis 1967; Belcher & MacGregor 1976; Cassinelli 1990) and later extended in all space around an axisymmetric system (Nerney & Suess 1975a,b,c, 1985; Sakurai 1985, 1987, 1990). The method employed by Nerney & Suess consists of a first order perturbative scheme of the spherically symmetric flow, relevant to solar wind theory where departures from radiality are expected to be small. On the other hand, Sakurai's treatment is a fully iterative numerical scheme. At the beginning, the split monopole geometry with radial fieldlines is prescribed. Then at each iteration, the momentum equation along the fieldline (Bernoulli) is solved while the transfield equation (Grad-Shafranov) is taken into account for a given flow along the pipe, although it is pointed out that both equations should be solved simultaneously. An analogous numerical technique has been developed by Li (1993) in the relativistic regime and for a pre-specified magnetic field line geometry. The analysis of Sakurai (1985, 1990) has also clarified the role of the classical critical points found by Weber & Davis (1967). Thus, the Bernoulli equation is shown to have two singularities for a *fixed* geometry, namely the slow and fast magnetosonic critical points, while in the transfield equation a singularity exists at the Alfvén transition. These critical points were shown by Heinemann & Olbert (Heinemann & Olbert 1978; Sakurai 1990) to correspond to some characteristic velocities (the speed of the cusp of the slow mode wavefront, the slow magnetosonic speed and the fast magnetosonic speed) wherein the transfield equation changes nature between the elliptical and hyperbolic one. Such a numerical treatment was the first to provide global solutions. Nevertheless, because of its pure numerical nature, only a few boundary conditions have been studied. Moreover, the streamlines do not converge to a cylindrical shape but rather to a paraboloidal one, very slowly and the cross section of the jet diverges only logarithmically. Thus the asymptotic speed is constant but the density drops to zero logarithmically as well. However the fieldline concentration near the polar axis forms a condensation along it instead of a hollow jet structure. This may be instable to the kink instability, as suggested there. A complementary numerical treatment has been performed for the time-dependent MHD equations resulting to a twisted hollow jet (Shibata & Uchida 1986, 1987). However, as it has been noted (Lovelace 1992) those models never reach a steady state and the twisting of the lines goes for ever.

Along the same lines, an analytical insight into the general properties of steady magnetized flows has been provided by analysing the asymptotic regime of the transfield equation for polytropic flows, although with the exception of isothermal flows (Heyvaerts & Norman 1989). There, it has been concluded that the behavior of the solution at the asymptotic regime depends crucially on the poloidal current enclosed. Conical asymptotics should enclose a finite constant poloidal current, but cannot carry it by themselves. On the other hand, paraboloidal asymptotics are shown to exist only in the case where the flow does not contain any poloidal current. Finally, it is shown that only cylindrical asymptotics are consistent with the polytropic MHD equations for a flow that is everywhere super fast magnetosonic. In particular, it is shown that the matching of external conical asymptotics to internal cylindrical asymptotics is not possible in a smooth way.

A *second* class studied so far are the so-called *self similar* models, or more precisely a class of scaling models where specific variable dependence has been assumed to allow analytical and/or simplified numerical work. Chan & Henriksen (1980) modelled axisymmetric and polytropic MHD flows in radio galaxies by neglecting gravity, setting to constants the MHD integrals of the mass flux per unit of magnetic flux and corotation angular frequency, truncating the Bernoulli integral, assuming transverse incompressibility, and finally assuming that all variables are separable in cylindrical coordinates (z, ϖ, φ) wherein the dependent variables have self-similar distributions across the flow. In particular, key-variables are ϖ-self-similar depending only on the vertical height z. Then, with an appropriately prescribed form of some external confining pressure, they observed numerically that the jet width exhibits quasi-periodic oscillations caused by an oscillation in the dominance of the external pressure and magnetic force on the one hand, and the internal pressure of the jet, on the other. Thus, this numerical analysis has revealed some interesting physical features, for example revealing an oscillatory shape of the jet. However, it suffers from the drawbacks of neglecting gravity and most important from the truncation of the Bernoulli integral wherein several ϖ^2-dependent terms are alltogether neglected. As a result, some not unimportant magnetic acceleration effects have been eliminated right from the beginning.

Another subclass within the self-similar models has been aimed towards an understanding of disk-winds (Blandford & Payne 1982) and recently generalized by Pelletier & Pudritz (1992). These centrifugally-driven wind solutions have been used extensively in relation with modelling the observations of collimated outflows from star forming systems (Pudritz & Norman 1983, 1986). In Blandford & Payne's (1982) analysis the variables are scaled with the spherical radius r instead of the cylindrical radius ϖ and the cold plasma approximation (no

thermal pressure gradient) is used in the limit of rapidly supersonic flows. Thus, for a fixed colatitude θ all physical quantities are equal within a factor of proportionality which is given at the disc surface. This method allows to reduce the set of the ideal MHD partial differential equations to a set of two ordinary differential equations in θ effectively. We may call these solutions r-self-similar since some key-physical quantities like the Alfvén number and the cross sectional area of all nested magnetic flux surfaces in units of the corresponding area at the Alfvén point, are solely functions of θ. A first order equation gives the evolution of the Alfvén number and another second order equation provides the field/streamline geometry. Both equations do possess the same singularities as a result of the simultaneous treatment of all components of the momentum equation. And consequently, apart from the Alfvén singularity, they find an extra critical point which is not the fast magnetosonic critical point. The Alfvén mode is an incompressible mode and thus is not affected, while the fast magnetosonic mode is shifted because waves must propagate orthogonally to the self-similar direction $\hat{\theta}$ and compressible wave amplitudes are modified accordingly in this direction. Actually, these solutions do not even pass through any critical point except the Alfvén singularity since the other X-type critical point is always rejected at infinite distance from the disc. Nevertheless they find two classes of solutions: one consists of fast magnetosonic solutions with paraboloidal asymptotics while the other one corresponds to transfastAlfvénic solutions with a turning point and focalisation onto the polar axis. Such a focalisation seemed to be unavoidable because of the current singularity along the axis in this model that creates an excess of pinching forces that neither the centrifugal forces nor the pressure gradient (that is neglected) can balance. However this result is rather surprising, because, if the flow remains superAlfvénic near the axis, the jet cross sectional area cannot be reduced to less than its Alfvénic value. In other words, centrifugal forces cannot be neglected near the rotational axis, even asymptotically. Pelletier & Pudritz's (1992) analysis is essentially solving the asymptotic fast magnetosonic regime in the cold plasma approximation, using a more general form of the scaling (i.e. using more general power laws). Although their solution is not self-similar, it still involves a partial differential equation, and not a complete decoupling of the variables. Among their solutions, they found one where the poloidal current does not diverge along the pole and at infinity. Yet these improved solutions correspond to a current free plasma where all the necessary poloidal current is concentrated along the polar axis, i.e., along a singular line of infinite current density. Thus the solution has to be cut at the inner edge of the disc. This was also required by the fact that the disc cannot be Keplerian close to the star. Consequently, another model is needed to explain the source of this inner current as well as the connection between the disc and the stellar wind. Blandford & Payne's (1982) r-self-similar solutions have been recently extended to cold relativistic flows by Li et al. (1992) showing that a kinetic energy flux comparable to, or higher than (Begelman & Li 1994) the Poynting flux can be achieved in these flows. On the other hand, Contopoulos & Lovelace (1993) seem to have extended the analysis of Blandford & Payne (1982) to more general power law dependences of the physical quantities and obtained various streamline shapes according to the magnitude of the poloidal current enclosed by a flux surface.

A *third* class of solutions has been studied by averaging the momentum equation across the jet and using an integral form of the transfield equation together with the Bernoulli equation. Two groups of studies which use this approach have been pursued. The narrow jet approximation (Koupelis & Van Horn 1990; Koupelis 1990) assumes that all quantities vary slowly across the jet such that they can be replaced by their average values. Obtaining thus an equation along the axis of the jet, it is further assumed that the jet has a constant opening angle. This last assumption, made for simplicity, seems to exclude solutions that reach high terminal values and the flow asymptotically is superAlfvénic but remains sub-fast magnetosonic with a decreasing velocity. Another group of studies which does not exhibits this drawback, assumes a separation of the variables and averages across the jet the various conservation laws (Lovelace et al 1992). Considering a hollow jet with the density and the toroidal magnetic field peaking at the edge of the jet, the jet does not carry any net poloidal current. They also assume that the jet is isothermal up to a certain distance above the Alfvén surface while it is adiabatic later on. The adiabatic region is consistently found by solving both the energy and the momentum equation while in the isothermal part a paraboloidal form of the line is assumed and fitted to cross the various critical points.

In previous articles we first studied the case of rotating hydrodynamic flows with a density enhancement at the equatorial regions and a streamline shape which is *prescribed* to be asymptotically radial (Tsinganos & Trussoni 1990); we found that the lighter plasma at the poles relative to the equator, together with a pressure higher at the equator than at the poles, resulted to high asymptotic speeds of the wind. In a similar rotating hydrodynamic outflow we indeed *deduced* this result that the streamlines become asymptotically radial throughout all of the meridional plane (Tsinganos & Sauty 1992, henceforth Paper I). The setting of these problems is motivated and the results are relevant to the phenomenon of fast streams associated with solar polar coronal holes. Radial asymptotically streamlines were also found in the subsequent study of a magnetized but nonrotating outflow for the unique wind-type solution that crosses several novel critical points (Tsinganos & Sauty 1993, henceforth Paper II). The case of rotating magnetized helicoidal outflows wherein the prescribed field line shape on the meridional plane was radial has been also analysed (Tsinganos & Trussoni 1992); there, the presence of the toroidal magnetic and velocity fields, in addition to the poloidal ones, were found to accelerate radially the outflow far from the base to high terminal speeds through the transfer of energy flux from the Poynting energy flux. However, a consequence of the assumed helicoidal structure is that, away from the base and the rotational axis, the large magnetic tension of the toroidal component requires, for transfield balance, a fast drop of the pressure as we move away from the magnetic axis, yielding thus a negative gas pressure at large angles from this axis. To avoid these negative pressures due to the radial

expansion of the poloidal field and flow of a helicoidal system we were guided to *prescribe* then a cylindrically collimated field pattern on the poloidal plane and for a system which in a first approximation was treated as nonrotating (Trussoni & Tsinganos 1993); the negative pressures were indeed avoided but due to the lack of available Poynting energy flux, the wind needed unrealistically high energies distributed throughout the entire length of the flow channel in order to escape in a collimated manner from the gravitational well. The natural following step is then to *deduce* the streamline shape in a rotating general MHD outflow; this is the subject of the present analysis.

The structure of our paper is then as follows. To establish our notation, in Sect. 2 we recall the basic integrals of the axisymmetric MHD equations for a singly ionized plasma flowing out of the gravitational potential of a central object. Then, Sect. 3 is dedicated to the physical characteristics of this model. In particular, we show how the general class of global solutions of this series of articles (Papers I & II) follows by judiciously choosing the functional dependence of the appropriate key physical quantities. It is emphasized that this class of global solutions is especially adapted to describe the close axis region of the flow in a consistent and general way. In Sect. 4 we examine the transfield equation and the Alfvénic transition in some detail. We then generalize the concept of the Bernoulli integral to our non-polytropic study and explore the superAlfvénic regime and the asymptotic conditions in Sect. 5. In particular, we show that the character of the asymptotic behaviour depends crucially on a characteristic parameter which measures the available magnetic rotator energy along the nonpolar streamlines as compared to the available energy along the polar axis. Thus, two classes of asymptotics are shown to exist, conical and cylindrical. In addition, collimated (cylindrical) solutions are shown to be characterized by oscillations whose wavelength is found in an analytical form by a simple expansion of the equations. And, those oscillations occur without the presence of an internal thermal pressure. In Sect. 6, we explore the subAlfvénic region and the problem of the topologies together with the critical points which choose the characteristic solutions. Thus, we are able to link the conditions at the Alfvén transition to the conditions at the source of the wind. Sect. 7 uses the global picture which emerges from Sects. 5 and 6 to illustrate the case of collimated solutions and a preliminary application to jets from T-Tauri stars is given. Such jets have two components, one rooted in the star and the other in the disc. The flow is shown to pass through three regimes: a thermally driven one, a magnetically driven one and finally an oscillating collimated regime wherein emission is likely to take place. In Sect. 8, we state a quantitative criterion for the transition from collimated jets to non collimated winds in terms of an anisotropy in the available input magnetic rotator energy. Basically we show that a wind may collimate into a jet if the available total volumetric Bernoulli energy is higher at the nonpolar streamlines than at the axis of rotation. A brief summary of our analysis together with some concludings remarks is finally given in Sect. 9.

2. Basic equations governing MHD outflows

In this section we write the conservation laws which govern our problem and briefly review their integrals when the system is axisymmetric.

2.1. Kinematics and energetics of MHD outflows

An astrophysical wind may be described to a first approximation as an inviscid and compressible plasma of infinite conductivity flowing out of the gravitational potential of a central object. The basic steady hydromagnetic equations governing the kinematics of this outflow are then,

$$\nabla \cdot \boldsymbol{B} = 0, \qquad \nabla \cdot (\rho \boldsymbol{V}) = 0\,, \tag{2.1a}$$

$$\nabla \times (\boldsymbol{V} \times \boldsymbol{B}) = 0 \qquad \Longleftrightarrow \qquad \boldsymbol{V} \times \boldsymbol{B} = \nabla \Phi\,, \tag{2.1b}$$

$$\rho(\boldsymbol{V} \cdot \nabla)\boldsymbol{V} = -\nabla P + \frac{1}{4\pi}(\nabla \times \boldsymbol{B}) \times \boldsymbol{B} - \frac{\rho \mathscr{G}\mathscr{M}}{r^2}\boldsymbol{e}_r\,, \tag{2.1c}$$

for the bulk flow speed $\boldsymbol{V}$, the magnetic field $\boldsymbol{B}$, the density ρ and the pressure P, with $\mathscr{M}$ denoting the mass of the central body, $\mathscr{G}$ the gravitational constant and r the spherical distance from the central object. Equations (2.1a) express magnetic flux and mass flux conservation while (2.1b) is the induction law for a plasma of high conductivity, also known as the frozen in condition and which at once can be integrated introducing thus the electric potential Φ. Finally, Eq. (2.1c) expresses the total momentum balance along the flow.

The above eight equations describe the kinematics of the outflow while the energetics should be described by the thermodynamic form of energy conservation, i.e., the first law of thermodynamics. Note that studies of cold plasmas (Blandford & Payne 1982; Pelletier & Pudritz 1992) have shown the possibility of accelerating jets with centrifugal forces. However, this requires a sufficient bending of the lines towards the disc and cannot account for the very initial step of the acceleration where the corona is strongly heated. Thus, the approach that we shall follow here is that for a wind to flow out of the gravitational well of a central object some sort of heating is needed – at least in the first stages of the outflow where it should dominate – in order to initiate the mass loss. We shall then denote the volumetric rate of such a thermal energy input by q with q positive(negative) in the case of a net heating(cooling). The crucial thermodynamic variable then is the heat content or enthalpy function h which represents the reservoir from where the gas in the wind absorbs thermal energy and converts it to kinetic energy,

$$q = \rho \boldsymbol{V} \cdot \left[\nabla h - \frac{\nabla P}{\rho}\right]\,. \tag{2.1d}$$

Evidently, in writing Eq.(2.1d) the volumetric enthalpy h is independent of any particular equation of state for the gas. On the other hand, by adopting the classical equation of state of perfect gases, which is certainly a good approximation for the astrophysical fluids that we are interested and for a ratio of the

specific heats in the gas $\Gamma = c_p/c_v$, this enthalpy function h takes the form,

$$h = \frac{\Gamma}{\Gamma - 1}\frac{k_B}{\mu}T, \qquad \text{with} \qquad \frac{k_B}{\mu}T = \frac{P}{\rho}, \tag{2.1e}$$

in terms of the temperature T, the reduced mass of the gas, μ, and Boltzmann's constant, k_B.

The system of equations (2.1) is mathematically closed for the eight unknown functions $(\boldsymbol{B}, \boldsymbol{V}, P, \rho)$ if q is known. However, the heating processes operating in the accelerating region of the gas in the astrophysical conditions of interest are usually poorly known and therefore a corresponding value for q is not available. Then, a polytropic relation between P and ρ is customarily assumed with a *constant* index $\gamma \neq \Gamma$ which effectively corresponds to an arbitrary form of the heating q (Weber & Davis 1967; Heyvaerts & Norman 1989; Sakurai, 1990). In this last case the enthalpy h is replaced by some effective enthalpy h',

$$h' = \begin{cases} \dfrac{\gamma}{\gamma - 1}\dfrac{P}{\rho} & (\gamma \neq 1) \\ c_s^2 \ln\rho & (\gamma = 1) \end{cases} \tag{2.1e}$$

where the case $\gamma = 1$ corresponds to an isothermal gas and c_s is the isothermal sound speed.

For a purely thermally driven wind, Parker (1963) has pointed out that enough supply of energy is necessary. Formally the polytropic index needs to be less than 3/2 in order to accelerate the flow out of the gravitational well of the central object. Of course a cut off could be introduced such that the flow becomes adiabatic on larger scales, once some magnitude of the velocity is reached. This idea has been explored recently in the case of noncollimated jets by Lovelace et al. (1991). A consequence of the above polytropic hypothesis is that solutions of the steady MHD equations are always characterized by the presence of three critical points, namely the slow, fast and Alfvén critical points. In this way, some important insight into the solutions of the complete set of the hydromagnetic equations and their properties is gained, albeit by sacrificing equally interesting insight and information on the energetics of the outflows. However, it is well known that a polytropic equation of state with *any* constant γ cannot yield correct values of the physical parameters of the solar wind, both close to the Sun and at 1 AU (Parker 1963). For example, the inadequacy of the polytrope law as a means of describing the energy equation can be seen by the fact that when someone tries to reproduce the observed conditions at 1 AU, unrealistically high velocities and unrealistically low densities near the solar surface are obtained (Weber & Davies 1967; Belcher & MacGregor 1976).

In the approach that we shall follow here, by means of an *a priori* physically sound choice of the streamline integrals, the MHD equations are explicitly solved without imposing any polytropic relation. Then, through the energy equation, the form of the heating/cooling distribution along the flow, q, is calculated *a posteriori* and *selfconsistently* with the assumed choice of the field and flow structure. In other words, instead of replacing a solution of the energy equation by a single parameter, γ, we replace it by a function, $q(R, \theta)$ [*cf.* Equation (2.1d)]. When compared with the approach of the polytropic equation of state, this approach has the advantage that by examining the energy function $q(R, \theta)$, we may decide if the assumed angular dependence of the physical quantities and the parameters used correspond to a physically acceptable solution (Tsinganos et al. 1992; Trussoni & Tsinganos 1993). The analytical nature of the study will also enable us to have a detailed display of the various complicated topologies of the MHD solutions for magnetized winds, an experience useful in more sophisticated numerical studies. It is interesting to also point out that the angular dependence of the physical quantities in the wind emerges naturally via an integration through a separation of the variables in the governing equations (2.1) (Lima & Priest 1993).

2.2. *Integrals of axisymmetric MHD outflows*

Axisymmetry allows a reduction of equations (2.1) in terms of conserved quantities along each magnetic field line. These free integrals are a consequence of the general properties of systems with an ignorable coordinate (Tsinganos 1982); consequently we shall follow the notations introduced there. It is convenient to use spherical coordinates (r, θ, φ) with φ denoting the toroidal or azimuthal angle, because of the spherical symmetry of the gravitational field. However, it may also be convenient to use cylindrical coordinates (ϖ, φ, z) because of the possibility of collimation of the flow along the axis z and the resulting cylindrical symmetry. In the following we shall use interchangeably the two notations keeping in mind that $\varpi = r\sin\theta$ and $z = r\cos\theta$. First we shall recall briefly some general results in order to introduce the necessary notations.

With axisymmetry, introduce a magnetic flux function A in terms of which define the poloidal magnetic field,

$$\boldsymbol{B}_p = \nabla \times \left(\frac{A}{r\sin\theta}\boldsymbol{e}_\varphi\right) = \frac{\nabla A}{\varpi} \times \boldsymbol{e}_\varphi, \tag{2.2}$$

and a streamfunction Ψ in terms of which define the field of the poloidal mass flux,

$$4\pi\rho\boldsymbol{V}_p = \nabla \times \left(\frac{\Psi}{r\sin\theta}\boldsymbol{e}_\varphi\right) = \frac{\nabla\Psi}{\varpi} \times \boldsymbol{e}_\varphi. \tag{2.3}$$

Then, due to axisymmetry and Eqs. (2.1), Ψ is constant on surfaces of constant A on which the corresponding streamlines and fieldlines are roped. Thus, the poloidal components of the velocity and magnetic fields are parallel to each other, $\Psi = \Psi(A)$ and we can write,

$$\boldsymbol{V}_p = \frac{\Psi_A}{4\pi\rho}\boldsymbol{B}_p, \tag{2.4}$$

where the subscript A indicates a derivative with respect to A. The total $\boldsymbol{V}$ and $\boldsymbol{B}$ are not aligned due to the existence of the electrical potential Φ in a rotating wind, but each surface of

constant magnetic flux is a surface of constant electrical potential, so $\Phi = \Phi(A)$. The toroidal component of the frozen flux condition, Eq. (2.1b), gives then

$$\frac{V_\varphi}{r\sin\theta} - \frac{\Psi_A B_\varphi}{4\pi\rho r\sin\theta} = \Phi_A = \Omega(A)\,, \tag{2.5}$$

where Φ_A is usually denoted by Ω to indicate that it has the dimensions of an angular speed and Eq. (2.5) is the so–called isorotation law because at the footpoints of each line on the disk or the star where the magnetic field dominates, their angular speed is equal to Ω [see Eq. (2.13)].

Another free integral is obtained by integrating the momentum equation in the azimuthal direction. It is usually denoted by $L(A)$ to indicate that it corresponds to the total angular momentum of the system fluid+field,

$$r\sin\theta\left(V_\varphi - \frac{B_\varphi}{\Psi_A}\right) = L(A)\,. \tag{2.6}$$

From the two previous equations we may derive the azimuthal components of the fields in terms of the free integrals $\Psi(A)$, $\Omega(A)$ and $L(A)$ (Tsinganos 1982). It is convenient to introduce the poloidal Alfvén number M, which is the ratio of the poloidal speed to the characteristic poloidal Alfvén speed,

$$M^2 = 4\pi\rho\frac{\boldsymbol{V}_p^2}{\boldsymbol{B}_p^2} = \frac{\Psi_A^2}{4\pi\rho}\,, \tag{2.7}$$

such that the azimuthal fields are,

$$B_\varphi = -\frac{L\Psi_A}{\varpi}\frac{1-\varpi^2\dfrac{\Omega}{L}}{1-M^2}\,, \qquad V_\varphi = \frac{L}{\varpi}\frac{\varpi^2\dfrac{\Omega}{L}-M^2}{1-M^2}\,. \tag{2.8}$$

2.3. Alfvén singularity

It is usually pointed out that these equations possess a singularity at the Alfvén point, when the density equals to the so-called Alfvén density $\rho_a(A)$ (using the subscript "a" to denote quantities evaluated at the Alfvén point, which should not be confused with the subscript "A" which denotes derivative with respect to A),

$$M^2 = 1 \quad\Longleftrightarrow\quad \rho(r,A)|_{M=1} = \rho_a(A) = \frac{\Psi_A^2}{4\pi}\,. \tag{2.9a}$$

To impose regularity, the two free functions L and Ω need to be related,

$$\varpi^2|_{M=1} = r^2\sin^2\theta|_{M=1} = \varpi_a^2(A) = \frac{L(A)}{\Omega(A)}\,, \tag{2.9b}$$

which introduces the Alfvénic cylindrical radius ϖ_a (noted sometimes by r_A in the litterature) as the ratio of the free integrals L and Ω and is therefore a function of A solely.

2.4. Generalized Bernoulli integral

Another constant of the motion may be obtained by integrating the equation of motion along each streamline. Projecting equation (2.1c) along a streamline or a fieldline (which is equivalent to project along the poloidal fieldline due to axisymmetry) one obtains after combination with (2.1d)

$$\rho\boldsymbol{V}\cdot\nabla E = q\,, \tag{2.10a}$$

where E is the sum of the kinetic, thermal, gravitational and Poynting energy flux densities,

$$E \equiv \frac{1}{2}V_{\rm p}^2 + \frac{1}{2}V_\varphi^2 + h - \frac{\mathscr{GM}}{r} - \frac{\Omega}{\Psi_A}r\sin\theta B_\varphi\,, \tag{2.10b}$$

In general E is not conserved along a fieldline because of the heating source q. However, one can still write the conserved quantity,

$$E - \int_{s_o}^{s}\frac{q(s,A)}{\rho(s,A)V_{\rm p}(s,A)}{\rm d}s = F(A)\,, \tag{2.10c}$$

where $F(A)$ is the generalized classical Bernoulli integral and s is the path length along a fieldline A.

2.5 Corotating frame and magnetic rotator energy

If at the base of the flow the poloidal Alfvén number is negligibly small, the rotational speed is from Eq. (2.5),

$$V_{\varphi,o} = \Omega(A)\varpi_o\,, \tag{2.11}$$

such that the angular velocities $\Omega(A)$ really represent the individual angular velocities of the roots of the fieldlines with the label A at the base. Furthermore, the physical significance of the angular velocity $\Omega(A)$ is that in a system which rotates with angular frequency $\Omega(A)$, the azimuthal velocity V'_φ is also parallel to the azimuthal magnetic field B_φ,

$$\boldsymbol{V}'_\varphi = V_\varphi - \Omega\varpi = \frac{\Psi_A}{4\pi\rho}\boldsymbol{B}_\varphi\,. \tag{2.12}$$

Thus, while in the inertial frame the flow makes a nonzero angle with the magnetic field such that the Poynting flux is finite,

$$\frac{S_z}{\rho V_z} = -\frac{\Omega}{\Psi_A}\varpi B_\varphi = \Omega L - V_\varphi\Omega\varpi\,, \tag{2.13}$$

in the corotating frame the flow is parallel to the magnetic field. Therefore, in this frame, there is no Poynting flux, $S' = 0$ but only the contribution of the centrifugal potential to the total energy E' which is,

$$E' \equiv \frac{1}{2}V_{\rm p}^2 + \frac{1}{2}(V_\varphi - \Omega\varpi)^2 + h - \frac{\mathscr{GM}}{r} - \frac{1}{2}\Omega^2\varpi^2 = E - \Omega L\,. \tag{2.14}$$

Note that there is some excess of energy in the inertial frame as compared to the corotating frame which equals to ΩL. It will be shown later that this energy plays an important role in determining the asymptotics of the outflow and will be called magnetic rotator energy, $E_{\rm MR}$.

In the following we turn our attention to the choice of the free integrals $\Psi(A)$, $\Omega(A)$, $L(A)$ and $F(A)$.

3. Physical characteristics of proposed model

Our goal in this section is to introduce the solutions which generalize the ones presented in Papers I and II, although in a somewhat different manner. These solutions are *global and exact* and all corresponding equations are solved simultaneously in all space. Nevertheless, they may be also obtained via a formal separation of the streamline coordinates A and R and subsequently a first order expansion in the governing equations (2.1) for axisymmetric systems.

3.1. Dimensionless variables

In order to facilitate the analysis it is convenient to use dimensionless variables starting with the Alfvén radius at the pole $r_\star$. At this radius the polar magnetic field, velocity and density are $B_\star$, $V_\star$ and $\rho_\star$, respectively, such that the Alfvén number at $r_\star$ is unity, while a dimensionless magnetic flux function α may be also introduced,

$$R = \frac{r}{r_\star}\,, \qquad \frac{B_\star^2}{4\pi\rho_\star} = V_\star^2\,, \qquad A = \frac{r_\star^2 B_\star}{2}\alpha(R,\theta)\,. \tag{3.1}$$

This normalization is generally used in the literature of magnetized rotating flows (Weber & Davies 1967; Sakurai 1985, 1987), although it is slightly different from the notation of our preceding Papers I and II wherein all quantities are normalized at the stellar base radius, r_o and the distance of a characteristic critical point r_x, respectively.

3.2. Shape of Alfvén surface

Our first crucial assumption relates to the shape of the Alfvén surface. In the absence of an accretion disk the shape of this surface emerges as ellipsoidal in the numerical modelling of Sakurai (1985); with an accretion disk present, the ellipsoidal form remains along the pole but it is distorted around the equator getting asymptotically a roughly conical shape (Sakurai 1987), similar to the one in the modelling of disk-winds by Blandford & Payne (1982). On the other hand, from a rather general perspective, it can be shown that a first order expansion in the asymptotically dominant magnetic pinching and centrifugal forces, in terms of the magnetic flux function A (*cf.* Eq. 5.11), is consistent with a spherical shape of the Alfvén surface. With these considerations in mind, then, it occurred to us that we may start our study by taking the Alfvén surface to be spherical such that the Alfvén number $M(R, A)$ depends on the spherical radius only and not on the particular fieldline,

$$M(R, A) = M(R)\,. \tag{3.2}$$

In other words, it is worth to emphasize that the above assumption (3.2) is consistent with our intuitive expectation that around the axis of the jet the flow has a rather spherical Alfvén surface, in any general and model-independent analysis; and, at the same time in the disk-wind region the Alfvén surface may obtain any other model-dependent shape. Thus, with (3.2) our modelling of the inner part of the jet is of a rather general character. On the other hand, the modelling of its outer part rooted into the disc may lack the generality of the inner region. Nevertheless, it is an exact solution which carries the memory of the modelling around the flow axis.

3.3. Separation of the variables in the density dependence

Because of the definition of the Alfvén number as the ratio of the Alfvén density $\rho_a(\alpha) = \Psi(\alpha)^2/4\pi$ and the density $\rho(R, \alpha)$, (Eq. 2.7), *the assumption of spherical Alfvén surfaces (3.2) automatically implies that the density should be taken in a separable form*, $\rho = \rho(R)\rho_a(\alpha)$ (*cf.* Eqs. 2.7-2.9a). Furthermore, we shall take only the first order term in an expansion of $\rho_a(\alpha)$ on α, $\rho_a(\alpha) = \rho_\star(1 + \delta\alpha)$ with δ a parameter describing deviations from a spherically symmetric density in this first order scheme. Note that this is the only consistent way to expand to first order in the magnetic flux function α the gravitational term in Eq. (2.1c). Thus, the density has the following form in terms of the Alfvén number and the magnetic flux function,

$$\rho(R, \alpha) = \frac{\rho_\star}{M^2(R)}(1 + \delta\alpha)\,. \tag{3.3}$$

The dependence of all other variables, such as the pressure and the azimuthal components of the fields will be discussed later in a consistent way with these assumptions.

3.4. Magnetic flux $F_{\rm mag}$

The form of the magnetosphere is determined by the explicit dependence of the magnetic flux function $\alpha(R, \theta)$ on its variables. If there exists a dead zone of closed fieldlines sandwiched at the equator by a region of open fieldlines, let the value of $\alpha(R, \theta)$ at the *last open* fieldline that encloses the flow region be $\alpha_{\rm out}$ and $A_{\rm out} = A(\alpha_{\rm out})$. Thus, at the reference "base" $r = r_\star$ these open fieldlines shall extend up to an angle $\theta_{\rm out}$ which of course shall depend on the particular form of $\alpha(R, \theta)$. For a given (α) the magnetic flux is conserved and the total magnetic flux $F_{\rm mag}$ — through an axisymmetric surface around the pole $\theta = 0$ where we assume that $\alpha = 0$ and extending up to the *last open* fieldline with the label $\alpha_{\rm out}$ on each hemisphere — is, using Stokes theorem,

$$F_{\rm mag} = \int\!\!\int_S \boldsymbol{B}_p \cdot \mathbf{dS} = 2\pi A_{\rm out} = \pi r_\star^2 B_\star \alpha_{\rm out}\,. \tag{3.4}$$

Note that *if* $\theta_{\rm out} = \pi/2$ such that at the "base" the surface S becomes all the northern hemisphere of area $S = \pi r_\star^2$, the flux through S is $F_{\rm mag} = \pi r_\star^2 B_\star$. Thus the meaning of the function A becomes apparent from the above equation: $2\pi A_{\rm out}$ represents the magnetic flux enclosed by some bounding axisymmetric fieldline $A_{\rm out}$.

Regarding the functional dependence of $\alpha(R, \theta)$ we first note that α can be developed in terms of multipoles. Taking into account the axial symmetry, we shall keep only the lowest possible terms in such an expansion writing,

$$\alpha(R, \theta) = f(R)\sin^2\theta\,. \tag{3.5}$$

In Eq. (3.5) the functional dependence of $f(R)$ reflects the degree of flow collimation. For example, $f(R)$ = constant means radial fieldlines while $f(R) \sim R^2$ corresponds to a cylindrical fieldline shape. Since we have normalized $f(R)$ to be 1 at $R = 1$, α varies from 0 at the pole to 1 at the equator. In other related studies, a specific form for f was chosen: $f(R) = 1 + c/R^n$ (Low & Tsinganos 1989), $f(R) = 1$ (Tsinganos & Trussoni 1990, 1991), $f(R) = 1 + cR^n$ with c a constant and n an integer (Trussoni & Tsinganos 1993). Here, as in Papers I and II, we shall not specify $f(R)$ but instead *deduce it a posteriori*.

Instead of using $f(R)$, in the present paper we find it more convenient to introduce the related function $G(R)$,

$$G(R) = \frac{R}{\sqrt{f}}$$

$$\Longleftrightarrow \qquad \alpha = \frac{R^2}{G^2(R)} \sin^2\theta = \frac{\varpi^2}{r_\star^2 G^2(R)}\,, \tag{3.6}$$

which measures the cylindrical distance to the polar axis of a flux tube limited by the magnetic line with the label α,

$$\varpi(R,\alpha) = \varpi_a(\alpha) G(R) \qquad \text{with} \qquad \varpi_a(\alpha) = r_\star\sqrt{\alpha}\,. \tag{3.7a}$$

The physical meaning of the function $G^2(R)$ is that it represents the cylindrical cross section of a flux tube, $S(R)$, normalized to its cross section S_a at the Alfvén point,

$$\frac{S}{S_a} = \frac{\varpi^2}{\varpi_a^2} = G^2(R)\,, \tag{3.7b}$$

Note that Eq. (3.5) is equivalent with the assumption of a separation of the variables in the function $\varpi^2(R,\alpha)$ of the cylindrical cross section of the jet, Eq. (3.7a); this separation of the variables is comparable to the one for the density, noting in addition that, as it was assumed for the Alfvén number, we have only taken the zeroth order term of the expansion of ϖ^2/ϖ_a^2 such that we have at the end all forces in the momentum balance equation expanded to first order. Then ϖ_a is expanded to first order, similarly to ρ_a in subsection 3.3, such that the Alfvén regularity condition (2.9b) is satisfied.

3.5. Expansion factor F

The logarithmic derivative of α with respect to the radius R is also physically meaningful. With α in a separable form, Eq. (3.5), it has already been suggested by the analysis of Paper II that an important function to be introduced is,

$$F(R) = \frac{\partial \ln \alpha(R,\theta)}{\partial \ln R} = \frac{R\mathrm{d}f}{f\mathrm{d}R} = 2\left(1 - \frac{\mathrm{d}\ln G}{\mathrm{d}\ln R}\right)\,, \tag{3.8}$$

which effectively measures the angle that the projection of a field line makes on the poloidal plane with the radial direction (see Paper II). Thus, $F = 2$ corresponds to cylindrical fieldlines, while $F = 0$ to radial fieldlines. Note that the asymptotic value of F at infinity is comparable to the parameter n used in Tsinganos & Trussoni (1993). We shall loosely call F the R-dependent expansion factor of the streamlines or simply the expansion factor.

3.6. Mass loss rate $\dot{M}$

First, it is worth to note that the free function $\Psi_A(\alpha)$ is,

$$\Psi_A(\alpha) = \frac{4\pi\rho_\star V_\star}{B_\star}\sqrt{1+\delta\alpha}\,, \tag{3.9}$$

which is a consequence of the choice made for the Alfvén density in subsection 3.3. Similarly to the magnetic flux, the poloidal mass flux can be defined in terms of the stream function Ψ. From Eq. (3.9), we have

$$\Psi(r,\theta) = 2\pi\rho_\star V_\star r_\star^2 \psi(\alpha)\,,$$

$$\psi(\alpha) = \int_0^\alpha (1+\delta\alpha')^{1/2}\mathrm{d}\alpha'\,, \tag{3.10}$$

such that mass is conserved. We find then for the mass loss rate $\dot{M}$ from each hemisphere of the star,

$$\dot{M} = \iint_S \rho\mathbf{V}_p\cdot\mathbf{dS} = \frac{\Psi_{\rm out}}{2} = \pi r_\star^2\rho_\star V_\star\psi(\alpha_{\rm out})\,, \tag{3.11}$$

with $\Psi_{\rm out} = \Psi(\alpha_{\rm out})$. Thus, we have for $\psi_{\rm out} \equiv \psi(\alpha_{\rm out})$,

$$\psi_{\rm out} = \begin{cases} \alpha_{\rm out} & (\delta = 0) \\ \dfrac{2}{3\delta}\left[(1+\delta\alpha_{\rm out})^{3/2} - 1\right] & (\delta \neq 0) \end{cases} \tag{3.12}$$

The ratio of the mass to magnetic flux from each hemisphere is then,

$$\frac{\dot{M}}{F_{\rm mag}} = \frac{\rho_\star V_\star}{B_\star}\frac{\psi(\alpha_{\rm out})}{\alpha_{\rm out}}\,. \tag{3.13}$$

The above expressions are still valid if we include lines that are not connected to the star (i.e., lines with labeling $\alpha > \alpha_{\rm out}$ possibly connected to a surrounding disk). Also, if the flow region extends from $\alpha_{\rm in}$ to $\alpha_{\rm out}$ instead from $\alpha_{\rm in} = 0$ to $\alpha_{\rm out}$ and we have a hollow jet emerging from an annular surface $S_{\rm ann.}$, the above expression for $\dot{M}$ can be modified accordingly,

$$\dot{M} = \iint_{S_{\rm ann.}} \rho\mathbf{V}_p\cdot\mathbf{dS} = \frac{\Psi_{\rm out} - \Psi_{\rm in}}{2}$$

$$= \pi r_\star^2\rho_\star V_\star\psi(\alpha_{\rm out},\alpha_{\rm in})\,, \tag{3.14}$$

with,

$$\psi(\alpha_{\rm out},\alpha_{\rm in}) = \begin{cases} \alpha_{\rm out} - \alpha_{\rm in} & (\delta = 0) \\ \dfrac{2}{3\delta}\left[(1+\delta\alpha_{\rm out})^{3/2} - (1+\delta\alpha_{\rm in})^{3/2}\right] & (\delta \neq 0) \end{cases} \tag{3.15}$$

Similarly to the magnetic flux function A, the meaning of the function Ψ becomes apparent in the above Eq. (3.11): $\Psi_{\rm out}/2$ represents the mass loss rate through the axisymmetric tube of open fieldlines around the pole which is bounded by the axisymmetric fieldline $\Psi_{\rm out}$. In the case of the annular flow region bounded by the streamlines with the labels $\Psi_{\rm in}$ and $\Psi_{\rm out}$, the difference $[\Psi_{\rm out} - \Psi_{\rm in}]/2$ represents the mass loss rate originating at the annular surface $S_{\rm ann.}$ where the streamlines with the labels $\Psi_{\rm in}$ and $\Psi_{\rm out}$ originate, Eq. (3.14).

3.7. Axial current I_z and total angular momentum loss rate $\dot{J}$

The two functions $L(A)$ and $\Omega(A)$ are free at the moment apart from their ratio L/Ω which is fixed by the regularity condition, Eq. (2.9b) and the choice expressed in Eq. (3.7a). To proceed with a consistent form for these two functions note that the total angular momentum loss rate $\dot{J}$ from each hemisphere of the star is,

$$\dot{J} = \int\int_S L(\alpha)\rho \mathbf{V}_p \cdot \mathbf{dS} = \frac{1}{2}\int_0^A L\Psi_A dA\,, \tag{3.16}$$

while the total axial current enclosed by a flux tube at a cylindrical radius ϖ is,

$$I_z = \frac{c}{2}\varpi B_\varphi = -\frac{c}{2}L\Psi_A \frac{1-\varpi^2/\varpi_a^2}{1-M^2} \approx -\frac{c}{2}L\Psi_A\,, \tag{3.17}$$

where the last approximation is at the stellar base where $M \approx 0$, $\varpi \ll \varpi_\alpha$. It follows that $L\Psi_A$ is a crucial function of our problem which expresses both the total angular momentum loss rate per unit of magnetic flux and the poloidal electric current carried by the outflow. Looking then for a general expression of $L\Psi_A$ which leads to solutions of the momentum equation in a separable form and at the same time the forces arising from the toroidal components of the fields are expanded to first order in A we find that to this order,

$$L\Psi_A = \lambda r_\star B_\star \sqrt{\alpha^2 + \mu\alpha}\,, \tag{3.18a}$$

where μ and λ are constants with λ describing the strength of the magnetic torque at $r_\star$. A careful examination of the consequences of this choice shows however that the angular velocity Ω would diverge at the pole unless $\mu = 0$. Although this is a characteristic of other models (see for example Blandford & Payne (1982) and Pelletier & Pudritz (1992) wherein the so called normal solution contains such a singularity), this case should be disregarded as an unphysical extension of those solutions near the flow axis. We prefer to find solutions without any singularity in the polar current demanding thus that $\mu = 0$. Then,

$$L\Psi_A = \lambda r_\star B_\star \alpha\,. \tag{3.18b}$$

In this way the poloidal current has been expanded to first order in A and it justifies our expansion to zeroth order in M^2 and ϖ^2/ϖ_a^2, if we constrain ourselves on expanding up to the first order only in the momentum equation. Note, however, that the solutions we obtain remain global and, at the same time, they are quite adapted to describe the inner part of the jet and the interplay of the anisotropic forces there. Then, with $\mu = 0$ we obtain the following forms for the total angular momentum per unit mass, L, the angular velocity of the corotating system Ω, and the total angular momentum loss rate $\dot{J}$ from each hemisphere of the star,

$$L(\alpha) = \lambda r_\star V_\star \frac{\alpha}{\sqrt{1+\delta\alpha}}\,, \qquad \Omega(\alpha) = \frac{\lambda V_\star}{r_\star}\frac{1}{\sqrt{1+\delta\alpha}}\,, \tag{3.19a}$$

$$\dot{J} = \frac{\lambda r_\star V_\star \dot{M}}{2}\frac{[\alpha_{\rm out}^2 - \alpha_{\rm in}^2]}{\psi(\alpha_{\rm out}, \alpha_{\rm in})}\,. \tag{3.19b}$$

Note that for $\delta = 0$, $\alpha_{\rm out} = 1$, $\alpha_{\rm in} = 0$ and we have a total angular momentum loss from both hemispheres, $\dot{J}_{\rm tot} = L\dot{M}$, i.e., the total angular momentum carried by the wind is equal to the product of the total mass loss rate and total angular momentum per unit mass, as expected. In general, this relation always holds with some filling factor as noted by Pudritz & Norman (1986).

3.8. Expressions of magnetic and velocity fields

The velocity and magnetic field can now be written exclusively in terms of unknown functions of R,

$$B_r = B_\star \frac{1}{G^2(R)}\cos\theta\,, \tag{3.20a}$$

$$B_\theta = -B_\star \frac{1}{G^2(R)}\frac{F(R)}{2}\sin\theta\,, \tag{3.20b}$$

$$B_\varphi = -B_\star \frac{\lambda}{G^2(R)}\frac{1-G^2(R)}{1-M^2(R)}R\sin\theta\,, \tag{3.20c}$$

$$V_r = V_\star \frac{M^2(R)}{G^2(R)}\frac{\cos\theta}{\sqrt{1+\delta\alpha(R,\theta)}}\,, \tag{3.20d}$$

$$V_\theta = -V_\star \frac{M^2(R)}{G^2(R)}\frac{F(R)}{2}\frac{\sin\theta}{\sqrt{1+\delta\alpha(R,\theta)}}\,, \tag{3.20e}$$

$$V_\varphi = V_\star \frac{\lambda}{G^2(R)}\frac{G^2(R)-M^2(R)}{1-M^2(R)}\frac{R\sin\theta}{\sqrt{1+\delta\alpha(R,\theta)}}\,. \tag{3.20f}$$

For later convenience we shall denote by N_B and N_V the numerator of B_φ and V_φ, respectively, which vanishes at the Alfvén point,

$$N_B = 1 - G^2\,, \tag{3.21a}$$

$$N_V = M^2 - G^2\,, \tag{3.21b}$$

while both components have the same denominator D,

$$D = 1 - M^2\,. \tag{3.21c}$$

3.9. Pressure dependence

Finally, the only remaining consistent choice for the pressure dependence is obtained by making again a first order expansion in terms of α

$$P(R,\alpha) = \frac{1}{2}\rho_\star V_\star^2 \Pi(R)[1 + K(R)\alpha]\,, \tag{3.22a}$$

a form similar to the one used in previous related studies (see Low & Tsinganos 1986; Tsinganos & Trussoni 1990, 1991; Trussoni & Tsinganos 1993; Papers I, II). We shall see later in Sect. 5.1 that this is the only choice consistent with equation (2.1c). For a given form of $f(R)$, we are led then to a system

of three equations for $\Pi(R)$, $K(R)$ and $M(R)$ as the three unknowns. However, here we shall follow the approach of Papers I and II where it is required that there exists the *same* heating profile along each streamline, putting thus $K = \kappa = \text{const.}$ (see Eq. 5.4a). In other words, this is equivalent to requiring that the effective polytropic index γ is the same function of R on each individual streamline. This demand then leads to a separable form for the pressure similar to that of the density,

$$P(R,\alpha) = \frac{1}{2}\rho_\star V_\star^2 \Pi(R)(1+\kappa\alpha)\,. \tag{3.22b}$$

Note that with this assumption the temperature profile is also the same along each streamline similarly to the heating rate. And, as with the case of the density, the deviations from a spherically symmetric pressure configuration are controlled by a single parameter, κ.

In the present paper similarly to the preceding paper II, we shall concentrate on a case which is even more simpler, wherein $\kappa = 0$ and

$$P(R,\alpha) = \frac{1}{2}\rho_\star V_\star^2 \Pi(R)\,, \tag{3.22c}$$

i.e., asumming that we can keep the zeroth order term in Eq. (3.22a) and the pressure is thus taken spherically symmetric. This assumption amounts to saying that pressure gradients across radial streamlines are neglected and only pressure gradients along the individual radial streamlines are taken into account. Note that this is an interesting intermediate case between flows described in the cold plasma approximation wherein pressure gradients are neglected alltogether and completely hydrodynamic flows confined by pressure gradients. We shall see in the following that even with such a simplifying assumption, the problem remains rather complicated and still contains the bulk physical characteristics of winds and jets.

Although in the present paper we shall treat explicitly only the case of Eq. (3.22c), we shall use Eq. (3.22b) in Sects. 4 and 5 to investigate some global properties of the problem without loss of generality and to also avoid in forthcoming papers going again through all general derivations. Thus, in Sect. 4 on the transfield equation and the regularity condition across the Alfvén surface we shall use Eq. (3.22b) and similarly in subsection 5.1 which treats the momentum equation along the field lines. However, from subsection 5.2 on, κ will be set equal to zero.

3.10. Gravitational potential

Before proceeding to Sect. 4, we need to define another dimensionless parameter of our model, ν, which represents the strength of the gravitational potential, $\mathscr{V}$, from which the wind escapes. It can be defined as the ratio of the escape speed at the Alfvén surface to the polar speed there, such that

$$\nu = \frac{V_{\rm esc}}{V_\star} = \sqrt{\frac{2\mathscr{G}\mathscr{M}}{r_\star V_\star^2}}\,. \tag{3.23a}$$

Then, the gravitational potential is,

$$\mathscr{V} = \frac{\mathscr{G}\mathscr{M}}{r} = \frac{1}{2}V_\star^2\frac{\nu^2}{R}\,. \tag{3.23b}$$

Note that since the gravitational potential $\mathscr{V}$ depends on the spherical distance R, it would be more convenient to use spherical coordinates close to the accelerating region of the flow where gravity is rather strong. On the other hand, cylindrical coordinates would be more appropriate to describe asymptotically an outflow which obtains the form of a collimated jet along the z-axis. Thus, oftentimes studies aimed at describing jet-type outflows neglect gravity because $\mathscr{V}$ has an inconvenient form in cylindrical coordinates which does not facilitate a separation of the variables (see e.g, Chan & Henriksen 1980). Since in this study we are interested for a complete solution from the accelerating region to infinity, including also the gravitational term, we shall use both types of coordinate description.

4. The transfield equation

In this section we discuss the equations which determine the shape of the streamlines and also some regularity conditions which need to be satisfied at the Alfvén transition of the flow. For the sake of generality of our arguments, in this section we shall include in our discussion the pressure gradient term across the fieldlines ($\kappa \neq 0$), according to the discussion in Sect. 3.9.

4.1. Equations determining the shape of the streamlines

By eliminating the angular-dependent terms in the momentum equation via the explicit angular dependences of the physical quantities presented in the preceding Sect. 3, one finds three independent equations for $\Pi(R)$, $F(R)$ and $M^2(R)$. Two of these arise from momentum-balance in the radial direction while the third from momentum-balance in the meridional direction. Thus, we obtain :

(1) the equation giving the derivative of the pressure,

$$\frac{\mathrm{d}\Pi}{\mathrm{d}R} + \frac{2}{G^4}\left[\frac{\mathrm{d}M^2}{\mathrm{d}R} + \frac{M^2}{R}(F-2)\right] + \frac{\nu^2}{R^2M^2} = 0\,, \tag{4.1a}$$

(2) the equation giving the derivative of the expansion function,

$$R\frac{\mathrm{d}F}{\mathrm{d}R} = \frac{\mathscr{N}_F(R,G,F,M,\Pi;\kappa,\delta,\nu,\lambda)}{\mathscr{D}(R,G,F,M;\kappa,\lambda)}\,, \tag{4.1b}$$

(3) the equation giving the derivative of the Alfvén number,

$$R\frac{\mathrm{d}M^2}{\mathrm{d}R} = \frac{\mathscr{N}_M(R,G,F,M,\Pi;\kappa,\delta,\nu,\lambda)}{\mathscr{D}(R,G,F,M;\kappa,\lambda)}\,. \tag{4.1c}$$

In the above system we have introduced for convenience the expressions:

$$\mathscr{D} = (M^2-1)\left(1+\kappa\frac{R^2}{G^2}\right) + \frac{F^2}{4} + R^2\lambda^2\frac{N_B^2}{D^2}\,, \tag{4.1d}$$

$$\mathcal{N}_F = -(\delta-\kappa)\nu^2\frac{RG^2}{2M^2}F$$
$$+\left(2\kappa\Pi G^2R^2+(F+1)(F-2)\right)\left(1+\kappa\frac{R^2}{G^2}-\frac{F^2}{4}-R^2\lambda^2\frac{N_B^2}{D^3}\right)$$
$$+\frac{M^2F}{4}(F-2)\left(F+2+2\kappa\frac{R^2}{G^2}+2R^2\lambda^2\frac{N_B^2}{D^3}\right)$$
$$-\lambda^2R^2F(F-2)\frac{N_B}{D^2}$$
$$+\lambda^2R^2\left(1+\kappa\frac{R^2}{G^2}-R^2\lambda^2\frac{N_B^2}{D^3}-\frac{F}{2}\right)\left(4\frac{N_B^2}{D^2}-\frac{2}{M^2}\frac{N_V^2}{D^2}\right). \tag{4.1e}$$

$$\mathcal{N}_M = (\delta-\kappa)\nu^2\frac{RG^2}{2M^2}(M^2-1)+\kappa\Pi R^2G^2M^2\frac{F}{2}$$
$$-\frac{M^4}{4}(F-2)(4\kappa\frac{R^2}{G^2}+F+4)$$
$$+\frac{M^2}{8}(F-2)(8\kappa\frac{R^2}{G^2}+F^2+4F+8)$$
$$-\lambda^2R^2(F-2)\frac{N_B}{D}$$
$$+\lambda^2R^2(2M^2+F-2)\left(\frac{N_B^2}{D^2}-\frac{1}{2M^2}\frac{N_V^2}{D^2}\right). \tag{4.1f}$$

The above set of equations gives the derivatives of Π, M^2 and F in terms of these unknown functions and $G(R)$ which is related to $F(R)$ through Eq. (3.8). Note that this casting of the system has two advantages. *First*, it is right away in a form immediately solvable by a Runge–Kutta numerical method; and *second*, it nicely reveals the role of those critical points obtained by putting equal to zero simultaneously the numerators and denominators of Eqs. (4.1b)-(4.1c).

We briefly note in passing that although the class of solutions discussed here are of rather different form from the self-similar ones discussed in Blandford and Payne (1982), it is remarkable that some formal similarities still exist between the two cases. Thus, we also have here an equation for the square of the Alfvén number M and one for the second derivative of the geometry function G exactly as their self similar solutions have one equation for the square of the Alfvén number (denoted by m) and a second order equation for the equivalent of the geometrical function (denoted by ξ). This general result is apparently independent of any particular assumption. Furthermore, by combining the momentum equation along a streamline with that across, one obtains those two equations where the same critical points appear at the denominators. However, the nature and location of those critical points shall of course depend on the details of the model into consideration, a point we discuss later.

4.2. The Alfvén regularity condition and the acceleration of the flow

As is well known, the Alfvén speed defined in terms of the poloidal magnetic field corresponds to the characteristic speed for the propagation of an incompressible mode in the plasma. At the location wherein the poloidal bulk flow speed equals to this Alfvén speed, a singularity appears in the azimuthal components of the hydromagnetic field as well as in the equations governing the poloidal field components (transfield equation), independently of the particular streamline geometry and the thermodynamics of the outflow. To treat properly this singularity, a condition is necessarily imposed at this Alfvén transition of the flow. Thus, in Sect. 2.2 by considering *first* the azimuthal components of the flow such a condition has been imposed between the two free integrals $L(A)$ and $\Omega(A)$ resulting to the requirement that when $M=1$, $G=1$ as well (*cf.* Eqs. 2.9a, 3.20c, 3.20f). Then, at the Alfvén transition denoted by a $\star$, B_φ and V_φ are given in terms of the finite ratio of the null quantities N_B and N_V,

$$\left.\frac{N_B}{D}\right|_\star \equiv \tau\ , \qquad \left.\frac{N_V}{D}\right|_\star = \tau-1\,. \tag{4.2}$$

Similarly, the acceleration of the flow (*cf.* Eq. 4.1c) is also finite at the Alfvén transition because $\mathcal{N}_M$ and $\mathcal{D}$ are also given in terms of powers of the finite ratios τ and $\tau-1$ and the presumably continuous function $F(R)$ across the Alfvén point. It is evident that as long as one works with a prescribed geometry wherein F is a continuous function of R (Weber & Davis 1967; Tsinganos & Trussoni 1991), the Alfvén transition does not correspond to a mathematical singularity and does not impose other requirements on the parameters of the flow (Sakurai 1985). The signature of this transition on the poloidal phase plane is the topology of a *star–point* from where "all solutions" pass, meaning that all slopes of the Alfvén number $M(R)$ are allowed on the plane $[M,R]$, as it has been demonstrated and illustrated in Tsinganos & Trussoni (1991).

The natural *second* step is then to calculate the undetermined forms $0/0$ of τ and $\tau-1$ which appear in the expressions of the azimuthal fields and the acceleration of the flow. Evidently, one can use l'Hospital's rule in order to get a relationship between the slope p in the $[M^2,R]$ plane and the undetermined ratio τ,

$$\tau = \left.\frac{\mathrm{d}G^2/\mathrm{d}R}{\mathrm{d}M^2/\mathrm{d}R}\right|_\star = \frac{2-F_\star}{p} \quad \text{where} \quad p\equiv\left.\frac{\mathrm{d}M^2}{\mathrm{d}R}\right|_\star . \tag{4.3}$$

Using this value of τ in the equation giving the acceleration of the flow as we get through the Alfvén point, a third order equation is obtained in p,

$$2F_\star p^3-(4\kappa\Pi_\star+F_\star^2-4-4\lambda^2)p^2$$
$$+8\lambda^2(F_\star-2)p-4\lambda^2(F_\star-2)^2=0\,. \tag{4.4}$$

When $\kappa=0$, by giving the values of $F_\star$ and λ, we obtain immediately the allowed slope of M at the Alfvén point and use it in order to numerically integrate across $R=1$. In the $\kappa\neq0$ case, on the other hand, the slope p depends in addition on the

value of $\Pi_\star$; however, this value can be fixed by demanding that the solution does not diverge asymptotically (*cf.* Paper I), and therefore the procedure is formally equivalent to the $\kappa = 0$ case which we shall illustrate in the present paper.

4.3. The Alfvén regularity condition and the shape of the streamlines

Note that so far no explicit use has been made of equation (4.1b), which describes the shape of the streamlines. However, we have implicitly used earlier Eq. (4.1b) by requiring that $F(R)$ is a continuous function of its variable across the Alfvén transition and thus obtained the above cubic (4.4) for p. Actually, a careful examination of the equation determining the streamline shape reveals that it contains the ratios of N_B and N_V with D. However, D appears at the denominator in a power higher by one than N_B and N_V do in the numerator of these ratios. Therefore, in order that the gradient $\mathrm{d}F/\mathrm{d}R$ does not diverge, one requires that $\mathcal{N}_F \cdot D = 0$ such that $\mathrm{d}F/\mathrm{d}R$ is finite when we have the form 0/0. This requirement that $\mathcal{N}_F \cdot D = 0$ yields then the following third order equation for τ,

$$\tau^3 + 2\tau^2 + \tau\left[\frac{\kappa\Pi_\star}{\lambda^2} + \frac{F_\star^2 - 4}{4\lambda^2} - 1\right] + \frac{(F_\star - 2)F_\star}{2\lambda^2} = 0\,. \quad (4.5)$$

The physical reason for demanding this condition is the requirement that the streamlines avoid a kink at the Alfvén transition, because a discontinuity in F means evidently a discontinuous change in the tangent of the angle to the fieldline (*cf.* Paper II Eq. 3.1). However, this last equation does not introduce an extra condition in the problem because it can be obtained by substituting Eq. (4.3) in Eq. (4.4). Of course this result is not surprising because Eq. (4.4) has been obtained by assuming a continuous $F(R)$.

It is interesting to note in passing that the requirement to impose an extra condition, such that the streamlines do not have a kink at the Alfvén point, has been originally emphasized by Sakurai (1985). However, the first quantitative expression of this condition has been given by Heyvaerts & Norman (1989). The cubic Eq. (39) derived in Appendix C of their paper by combining Eqs. (C.8) and (C.9) is indeed in the case of polytropic winds the corresponding equation of our cubic Eq. (4.4), if we note that our p is related with theirs (p_{HN}) in Eq. (C.9) by the relation $p_{\mathrm{HN}} = 1 + p/2$.

Let us now turn our attention to a parametric study of the regularity condition we have presented here.

4.4. Parametric illustration of the Alfvén regularity condition

To get an idea of the parametric dependence of the regularity condition at the Alfvén point and establish some connection with the nonrotating study of Paper II, in Figs. 1(a-d) we plot the slope p of the square of the Alfvén number $M^2(R)$ as a function of $F_\star$, for four representative values of $\lambda = 0, 0.1, 1,$ and 10.

Consider *first*, the limit of no rotation ($\lambda = 0$), studied in detail in Paper II. In this special case the cubic Eq. (4.4) has only a single root of finite value p while the other two collapse to the degenerate value $p = 0$ which is unphysical because in that case τ becomes infinite. The allowed values of $F_\star$ are around $F_\star = 0$ and in particular $F_\star \in [-2, 2]$. For $F_\star < 0$ we have $p > 0$ and the solution is accelerating at the Alfvén point corresponding to a wind or jet-type outflow. On the other hand, when $F_\star > 0$, we get $p < 0$ corresponding to the case of a decelerating outflow at the Alfvén point, or an accretion-type flow. The cases studied in Paper II were for accelerating outflows corresponding to $p > 0$ and $F_\star < 0$, with $F_\star$ approaching to zero from negative values and p ever increasing as the values of the density parameter δ increased. This is shown in Fig. (1a) wherein for $F_\star < 0$, p is positive and increases as $|F_\star| \to 0$. In this case of no rotation the Alfvénic transition is no longer a singularity and one passes smoothly from the subAlfvénic regime to the superAlfvénic while the streamlines become asymptotically radial.

Second, for the rotating case of $\lambda \neq 0$, the experience gained by the study of the nonrotating case of Paper II would suggest that, similarly, the most interesting range of F values should be around $F_\star = 0$. Indeed, as we shall illustrate in the following Sect. 6, this range is the most physically interesting one because then the topology of the solutions contains an X-type critical point which selects a unique physical solution, as in Paper II. Then, and once rotation sets in, two extra roots emerge in the range $F_\star \in [-2, 2]$. Since winds and jets always involve a transition from subAlfvénic (upwind) to superAlfvénic (downwind) regimes, they correspond to the accelerating at the Alfvén point solutions wherein $p > 0$ while all $p < 0$ correspond to accretion-type flows. Since our interest here is confined on jet-type outflows, among all possible solutions only those having a positive slope p will be considered. Further, we note that when $F_\star > 2$ the outflow is already collimated more than cylindrically at the Alfvén point and the flow channel area is less than $\pi\varpi_a^2$; those jets are collimated too close to the base (see Sect. 4). Of the two values of p for $F_\star < 0$, the larger is on the upper branch and reaches unrealistically large values corresponding to an almost null values of τ; the second positive root lies in the lower branch which is just above the axis $p = 0$ and becomes of interest when λ is large enough. In the following section we shall see how the only physically interesting solution jumps with the increase of the rotation parameter λ from the upper branch to the lower.

It is evident that a transAlfvénic solution will remain superAlfvénic or subAlfvénic once it crosses the line $M = 1$ satisfying the regularity condition. Then, one can study separately the topology in each regime. In the following Sect. 5 we first study the superAlfvénic regime using the Bernoulli integral; then in Sect. 6 the subAlfvénic regime which contains the second X-type critical point is studied in more detail.

5. The Bernoulli integral and conditions in the superAlfvénic asymptotic regime

In this section we discuss the Bernoulli integral and how this can be used to determine the outflow conditions at very large

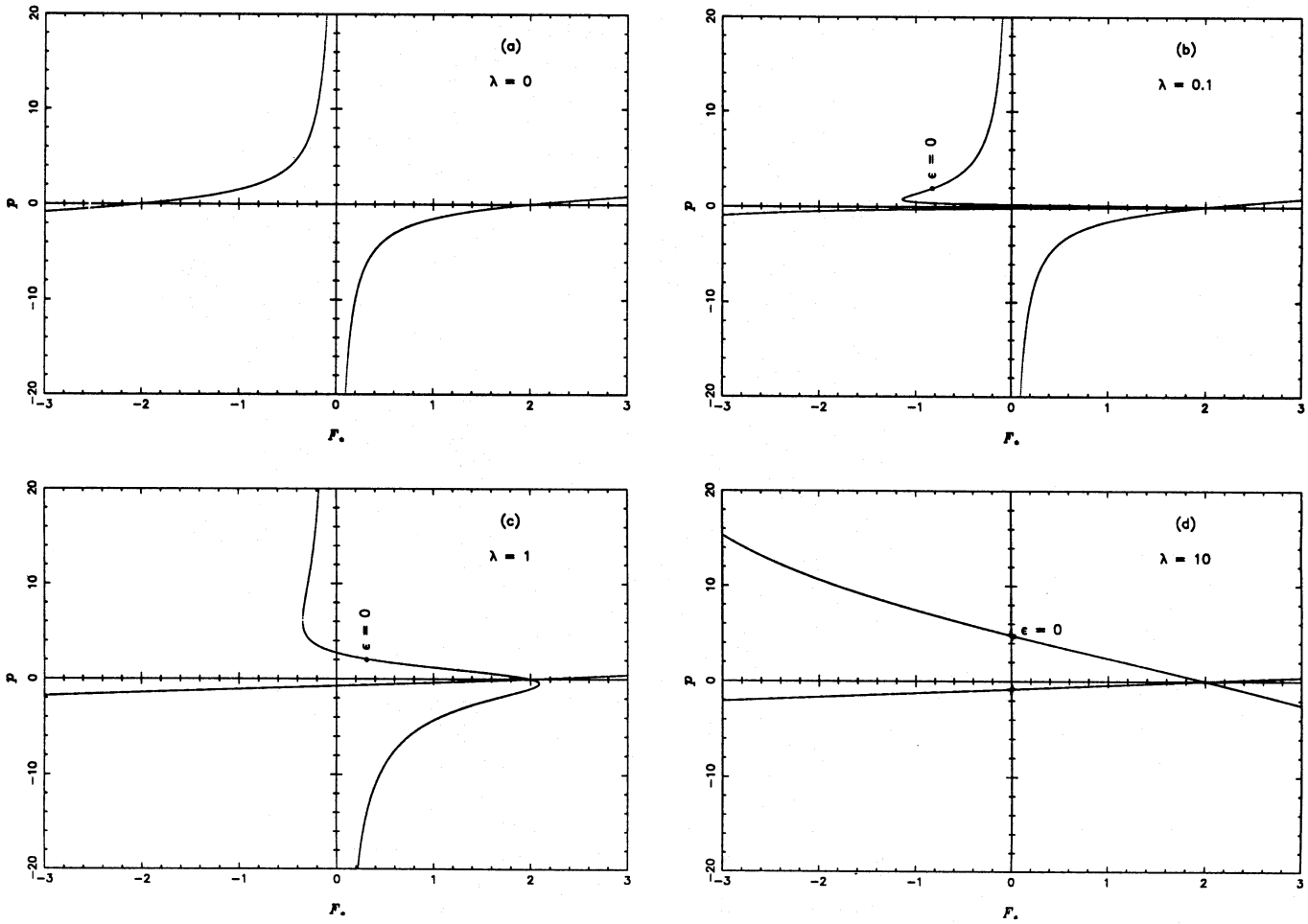

Fig. 1a–d. Plot of the slope p of the squared Alfvén number, $M^2(R)$, across the Alfvén singularity, as a function of $F_\star$. The solution of the cubic (4.4), in the case $\kappa = 0$, is given for four different values of the rotational parameter λ: $\lambda = 0$, in **a**, $\lambda = 0.1$, in **b**, $\lambda = 1$ in **c** and $\lambda = 10$ in **d**. We mark with a • the Alfvénic point of the critical solutions for $\epsilon = 0$, used in Sect. 6

distances from the origin. We discuss also some general properties of collimated flows along their axis which seem to be of a rather general physical nature.

5.1. Energy flux and the Bernoulli integral ϵ

Considering the above assumptions and the general relation for the pressure given by Eq. (3.22a), the rate of heating has the following form,

$$\frac{q(R,\theta)}{\rho(R,\theta)V_r(R,\theta)} = \frac{V_\star^2}{2r_\star}\frac{\mathscr{Q}_1(R)+\mathscr{Q}_2(R)\alpha}{1+\delta\,\alpha}\,, \tag{5.1a}$$

where the dimensionless quantities $\mathscr{Q}_1$ and $\mathscr{Q}_2$ are,

$$\mathscr{Q}_1(R) = \frac{1}{\Gamma-1}\left[M^2\frac{\mathrm{d}\Pi}{\mathrm{d}R}+\Gamma\Pi\frac{\mathrm{d}M^2}{\mathrm{d}R}\right]\,, \tag{5.1b}$$

$$\mathscr{Q}_2(R) = \frac{\beta^2}{\Gamma-1}\left[M^2\frac{\mathrm{d}}{\mathrm{d}R}(K\Pi)+\Gamma K\Pi\frac{\mathrm{d}M^2}{\mathrm{d}R}\right]\,. \tag{5.1c}$$

Next, consider the sum of the kinetic, thermal, gravitational, and Poynting energy flux densities per unit of mass flux density, denoted by E in Eq. (2.10b),

$$E = \frac{V_\star^2}{2}\frac{\mathscr{E}_1(R)+\mathscr{E}_2(R)\alpha}{1+\delta\,\alpha}\,, \tag{5.2a}$$

where

$$\mathscr{E}_1(R) = \frac{M^4}{G^2}+\frac{\Gamma}{\Gamma-1}\Pi M^2-\frac{\nu^2}{R}\,, \tag{5.2b}$$

and

$$\mathscr{E}_2(R) = \frac{M^4}{R^2G^2}\left[\frac{F^2}{4}-1\right]+\frac{\Gamma}{\Gamma-1}K\Pi M^2-\frac{\delta\,\nu^2}{R} + \frac{\lambda^2}{G^2}\left[\frac{M^2-G^2}{1-M^2}\right]^2+2\lambda^2\left[\frac{1-G^2}{1-M^2}\right]\,. \tag{5.2c}$$

The energy E is not conserved along a certain streamline α = constant because of the input of thermal heating expressed by the fact that $q(R,\theta)\neq 0$. However, by subtracting this thermal

heating as in Eq. (2.10c), the remaining part is conserved along a particular streamline,

$$\frac{\left[\mathscr{E}_1(R) - \int_{R_o}^{R} \mathscr{Q}_1(R)dR\right] + \left[\mathscr{E}_2(R) - \int_{R_o}^{R} \mathscr{Q}_2(R)dR\right]\alpha}{1+\delta\alpha} \equiv$$

$$\mathscr{F}(\alpha) = \frac{\mathscr{F}_1 + \mathscr{F}_2\alpha}{1+\delta\alpha}\,. \tag{5.3a}$$

where $F = (1/2)V_\star^2\mathscr{F}(\alpha)$ and $\mathscr{F}_1$, $\mathscr{F}_2$ are real constants. It follows that

$$\mathscr{E}_1(R) - \int_{R_o}^{R} \mathscr{Q}_1(R)dR = \mathscr{F}_1\,, \tag{5.3b}$$

and

$$\mathscr{E}_2(R) - \int_{R_o}^{R} \mathscr{Q}_2(R)dR = \mathscr{F}_2\,. \tag{5.3c}$$

Note that by taking the derivative with respect to R in Eq. (5.3b) we obtain the r-component of momentum balance. Also, we should keep always in mind that the above integrals are taken along a streamline α = constant. This last constrain halts further progress as long as we keep the general form of Eq. (3.22a) and the two integrals in Eq. (5.3) are uncorrelated. However, by making the extra assumption of equation (3.22b), $\mathscr{Q}_1$ and $\mathscr{Q}_2$ become proportional to each other,

$$\mathscr{Q}_2 = \kappa\mathscr{Q}_1 \quad\Longleftrightarrow\quad q(R,\alpha) = q(R,0)\cos\theta\frac{1+\kappa\alpha}{(1+\delta\alpha)^{1/2}}\,, \tag{5.4a}$$

and the two integrals are identical within a factor κ. The same happens to the heating terms in Eqs. (5.3) and therefore we may eliminate Π from the expressions of $\mathscr{E}_1$ and $\mathscr{E}_2$ in Eqs. (5.1b-5.1c) by forming the difference, $\epsilon = \mathscr{E}_2 - \kappa\mathscr{E}_1$. Thus, by multiplying Eq. (5.2b) by κ and subtracting it from Eq. (5.2c), it is easy to show that

$$\frac{\mathrm{d}}{\mathrm{d}R}\left[\mathscr{E}_2 - \kappa\mathscr{E}_1\right] = \mathscr{Q}_2 - \kappa\mathscr{Q}_1 = 0\,, \tag{5.4b}$$

and therefore the quantity ϵ is a constant for *all* streamlines,

$$\epsilon \equiv \mathscr{E}_2 - \kappa\mathscr{E}_1 = \mathscr{F}_2 - \kappa\mathscr{F}_1$$
$$= \frac{M^4}{(GR)^2}\left[\frac{F^2}{4} - 1 - \kappa\left(\frac{R}{G}\right)^2\right] - \frac{(\delta-\kappa)\nu^2}{R}$$
$$+ \frac{\lambda^2}{G^2}\left(\frac{N_V}{D}\right)^2 + 2\lambda^2\frac{N_B}{D}\,. \tag{5.5a}$$

Combining (5.4b) and (5.3a) the total conserved flux of energy along each streamline is

$$\mathscr{F}(\alpha) = \frac{\mathscr{F}_1 + (\kappa\mathscr{F}_1 + \epsilon)\alpha}{1+\delta\alpha}\,. \tag{5.5b}$$

Evidently, the choice of the pressure dependence we made on R and θ is the unique choice that leads to a Bernoulli-type energy equation along each streamline. The new constants ϵ and $\mathscr{F}_1$ are independent of the particular streamline, a fact consistent with the corresponding assumption that the effective polytropic index γ (see Paper II for its definition) is chosen independently of the fieldline to be a function of R alone. This result could have been presented as the initial assumption from which we could have deduced the pressure θ-dependence of Eq. (3.22b).

$\mathscr{F}_1$ can be evaluated at R_o where it corresponds to $\mathscr{E}_1(R_o)$ so it will depend on the initial pressure of the wind. To assign a physical meaning to ϵ, note that in the special case $\kappa = 0$ which we treat in this article, we have

$$\epsilon = \frac{\Psi_A^2(\alpha)F(\alpha) - \Psi_A^2(\mathrm{pole})F(\mathrm{pole})}{(1/2)V_\star^2\alpha\Psi_A^2(\mathrm{pole})}$$
$$= \frac{\rho(r,\alpha)F(\alpha) - \rho(r,\mathrm{pole})F(\mathrm{pole})}{(1/2)V_\star^2\alpha\rho(r,\mathrm{pole})}\,. \tag{5.6}$$

Thus, the sign of ϵ determines whether there is a deficit of energy per unit volume (and not per unit mass) along the polar streamline as compared to the other streamlines (case $\epsilon > 0$) or, an excess of energy in the polar streamline as compared to the other nonpolar streamlines (case $\epsilon < 0$). The last form shows that the role played by ϵ can be easily generalized to other models through its relationship with $F(\alpha)$. Equation (5.5b) makes also evident that our procedure indeed is equivalent to expand ρF to first order in α, a point related to the fact we already have mentioned, namely that the momentum equation is expanded to first order in α.

In the more often used polytropic approach, an artificial form of the heating is effectively prescribed by fixing the value of the polytropic index γ. The present study can be regarded as a step forward from this polytropic case towards a more general form for the relation between pressure and density; our only assumption short of any such general pressure-density relation is that we have assumed that the pressure radial profile is the same on each streamline to a multiplying factor depending on the line only. Also, the existence of a conserved quantity (ϵ) despite that no polytropic relation has been imposed, is interesting because it allows some analytical insight into the equations. It will turn out to be in our model of crucial importance in controlling the asymptotics. In addition however, such an approach can be extended to models with a Bernoulli-type energy equation – in which case ϵ should remain a conserved quantity along each line – and to other cases with more complicated heating functions. Then it would be interesting to see how the excess, or deficit of energy, along the pole compared to the other streamlines is crucial in controlling the collimation of the outflow.

From this point on, only the simpler form of equation (3.22c) ($\kappa = 0$) will be used throughout the rest of this paper. However, we have seen here that some of the basic features treated in the limit of a spherically symmetric pressure can be easily extended to a more general class of solutions which take into account a nonspherically symmetric pressure distribution.

5.2. *Asymptotic conditions*

Using cylindrical coordinates, the azimuthal components of the fields become,

$$B_\varphi = -\lambda B_\star\frac{\varpi}{r_\star G^2}\left(\frac{1-G^2}{1-M^2}\right)\,, \tag{5.7}$$

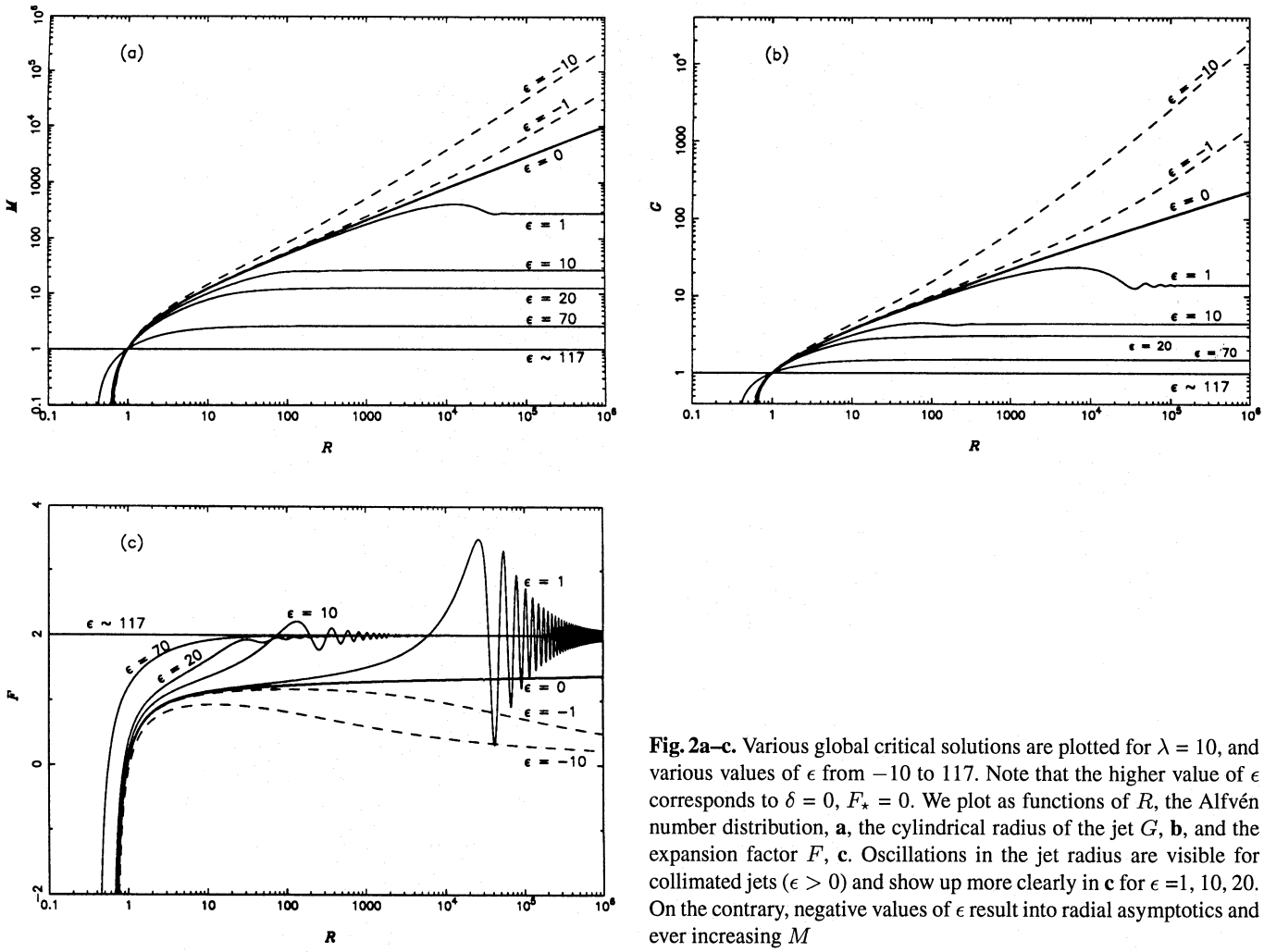

Fig. 2a–c. Various global critical solutions are plotted for $\lambda = 10$, and various values of ϵ from -10 to 117. Note that the higher value of ϵ corresponds to $\delta = 0$, $F_\star = 0$. We plot as functions of R, the Alfvén number distribution, **a**, the cylindrical radius of the jet G, **b**, and the expansion factor F, **c**. Oscillations in the jet radius are visible for collimated jets ($\epsilon > 0$) and show up more clearly in **c** for ϵ =1, 10, 20. On the contrary, negative values of ϵ result into radial asymptotics and ever increasing M

$$V_\varphi = \lambda V_\star \frac{\varpi}{r_\star G^2} \frac{1}{\sqrt{1+\delta\,\alpha}} \left(\frac{G^2 - M^2}{1 - M^2} \right) . \tag{5.8}$$

For a collimated outflow (jet), as $R \longrightarrow \infty$, $F \longrightarrow 2$ and the first two terms in Eq. (5.5a) due to deviations from full collimation and gravity disappear. Then, the Bernoulli constant ϵ takes the simpler form,

$$\epsilon = \frac{\lambda^2}{(M_\infty^2 - 1)^2} \left[\frac{(M_\infty^2 - G_\infty^2)^2}{G_\infty^2} + 2(M_\infty^2 - 1)(G_\infty^2 - 1) \right] , \tag{5.9}$$

where the Alfvén number M and the cylindrical radius factor G take their asymptotic values, M_∞ and G_∞, respectively. Therefore, for the collimated superAlfvénic outflow, it follows that ϵ is positive.

In the absence of rotation, the sign of ϵ is determined by the first term in Eq. (5.5a). Thus, in paper II, physical solutions were obtained for $\epsilon < 0$ and were shown to be non collimated, becoming conical asymptotically. There is only one special case wherein collimation is obtained asymptotically, occurring when $\epsilon = 0$.

If rotation is too small at the Alfvén surface, $\epsilon > 0$ cannot be achieved because the flow is almost radial there (see Paper II and subAlfvénic topologies in Sect. 6) unless we have a very negative δ which is also known to correspond to decelerating flows (see Tsinganos & Vlastou 1988; Low & Tsinganos 1989; Tsinganos & Trussoni 1991; Papers I and II). We discuss in Sect. 8 how it is possible to find numerically that the flow becomes radial asymptotically, recovering there the analytical solution of Paper I. Let us now consider the case where the boundary conditions are such that we really have a focusing of the streamlines into cylinders.

Switching to the cylindrical coordinates (z, ϖ, ϕ), the fields have only z– and ϕ–components when the flow is collimated; their z-components are constant while their ϕ–components are $B_\varphi = B_\varphi(\varpi)$ and $V_\varphi = V_\varphi(\varpi)$, Eqs. (5.7-5.8). Momentum balance in the ϖ–direction of the cylindrical radius ϖ is expressed then by,

$$\frac{\rho V_\phi^2}{\varpi} = \frac{\mathrm{d}}{\mathrm{d}\varpi} \left[\frac{B_\phi^2}{8\pi} \right] + \frac{B_\phi^2}{4\pi\varpi} . \tag{5.10}$$

The above equation simply states the fact that the outwards centrifugal force due to rotation is completely balancing the sum

of the inwards magnetic pinching force and the inwards gradient of the magnetic pressure which is built up by the increasing with the cylindrical distance ϖ strength of B_ϕ.

In the present model with κ=0 the pressure gradient balances asymptotically the gravitational term (because of the splitting of the equations) exactly and both vanish asymptotically, with the pressure becoming a constant. As a matter of fact Eq. (5.10) can be also obtained by taking the dominant terms in Eqs. (2.1) assuming that collimation is reached.

Thus, Eq. (5.10) yields the following relation between G_∞ and M_∞,

$$(M_\infty^2 - G_\infty^2)^2 = 2M_\infty^2(1 - G_\infty^2)^2 . \tag{5.11}$$

Solving this for G_∞ as a function of M_∞ we find two solutions

$$G_\infty^2 = M_\infty \frac{\sqrt{2} \pm M_\infty}{\sqrt{2}M_\infty \pm 1} . \tag{5.12}$$

The $\pm$ has to be chosen according to the value of M_∞ such that G_∞^2 remains positive. Practically, interesting solutions with $G_\infty > 1$ and $M_\infty > 1$ are obtained by taking the plus sign. Substituting G_∞ in Eq. (5.9) we find M_∞ as a function of ϵ/λ^2,

$$M_\infty = \sqrt{2}\left[\frac{2\lambda^2}{\epsilon} - 1\right] . \tag{5.13}$$

When this value of M_∞ as a function of (ϵ/λ^2) is substituted in Eq. (5.11) we obtain the cylindrical radius function G_∞ in terms of (ϵ/λ^2)

$$G_\infty^2 = \frac{4\lambda^2}{\epsilon}\left(\frac{2\lambda^2/\epsilon - 1}{4\lambda^2/\epsilon - 1}\right) . \tag{5.14}$$

In order to get some physical insight from these relations, note that the value of G_∞ is reflecting to us information about the asymptotical value of the cylindrical radius of the jet. Consider the last open streamline of the flow tube with the label $\alpha_{\rm out}$. Denote by ϖ_∞ the cylindrical radius of the jet (i.e., the cylindrical distance to the flow axis of the last open fieldline at $R \longrightarrow \infty$). Then

$$\frac{\varpi_\infty}{\varpi_a} = G_\infty , \tag{5.15}$$

where ϖ_a is the cylindrical radius at the Alfvén point.

Let us keep fixed the parameter λ and consider some characteristic values of the above expressions when ϵ varies. *First* note that when $\epsilon = 0$, $G_\infty = \infty$, and $M_\infty = \infty$. The streamlines become cylindrical asymptotically but the outflow expands all the way long. At the same time the asymptotical velocity is infinite. To see it notice that

$$V_\infty = V_\star \frac{M_\infty^2}{G_\infty^2} = V_\star \frac{\epsilon}{2\lambda^2}\left(\frac{2\lambda^2}{\epsilon} - 1\right)\left(\frac{4\lambda^2}{\epsilon} - 1\right) . \tag{5.16}$$

Then as ϵ increases G decreases while the Alfvén number M_∞ and the final velocity decrease. An upper limit exists in the value of ϵ for a given λ because the flow must remain superAlfvénic, so $M_\infty > 1$. This limit is reached when $\epsilon \longrightarrow \epsilon_{\rm max} = 2\lambda^2(2-\sqrt{2})$, then $M_\infty \longrightarrow 1$ and $G_\infty^2 \longrightarrow 1$.

In Figs. (2a, 2b) we have plotted $M(R)$ and $G(R)$ for a fixed value of λ, say $\lambda = 10$ and several values of ϵ between 0 and the maximum value $2\lambda^2(2 - \sqrt{2})$,

$$\begin{cases} \epsilon = & -10, & -1, & 0, & 1, & 10, & 20, & 70, & 117 \\ \varpi_\infty/\varpi_a = & \infty, & \infty, & \infty, & 14, & 5.4, & 3, & 1.5, & 1 \end{cases}$$

such that the above analytical results can be verified in the asymptotical limit.

5.3. Oscillations in the quasi-asymptotic regime of collimated jets

In this section we assume again that the pressure is spherically symmetric ($\kappa = 0$) and that collimation in the flow is obtained. From the previous section we know that the asymptotic quantities in the flow are uniquely determined by the initial value of ϵ/λ^2 which is a constant along all fieldlines.

An expansion of G and M can be made then to get an idea of the fluctuations that exist far from the region of the initial acceleration of the wind,

$$G^2 = G_\infty^2(1 + \theta) , \tag{5.17a}$$

$$M^2 = M_\infty^2(1 + \mu) , \tag{5.17b}$$

where θ, $\mu \ll 1$. Then we may similarly expand F to first order in Eq. (3.8),

$$F = 2 - R\dot{\theta} , \tag{5.18a}$$

while the derivative of F can be also expanded at large R as,

$$R\frac{{\rm d}F}{{\rm d}R} = R\dot{\theta} - R^2\ddot{\theta} \approx -R^2\ddot{\theta} . \tag{5.18b}$$

Thus keeping only the dominant term in Eq. (4.1b) one finds,

$$\frac{{\rm d}F}{{\rm d}R} = -2\lambda^2 \frac{R}{D^3}\left(2N_B^2 - \frac{N_V^2}{M^2}\right) , \tag{5.19}$$

which can be again expanded to first order. Since to zeroth order the RHS of this equation is zero and the LHS is condition (5.11) that we examined in the previous section, the remaining first order terms give a first relation between $\ddot{\theta}$, θ and μ

$$\ddot{\theta} = -2\lambda^2\left[\frac{2G_\infty^2}{(1 - M_\infty^2)^2}\left(\frac{1 - G_\infty^2}{1 - M_\infty^2} + \frac{G_\infty^2}{M_\infty^2}\right)\theta + \frac{M_\infty^4 - G_\infty^4}{(1 - M_\infty^2)^3 M_\infty^2}\mu\right] . \tag{5.20}$$

This can be combined with the Bernoulli equation (5.5a) that we also expand to first order – where again the zeroth order is Eq. (5.9) – to get a relation between μ and θ

$$\mu = \left[M_\infty^4 + G_\infty^4(1 - 2M_\infty^2)\right]\frac{1 - M_\infty^2}{2M_\infty^4(1 - G_\infty^2)^2}\theta . \tag{5.21}$$

Finally, by eliminating μ from Eqs. (5.20)-(5.21), an equation is obtained similarly to the classical harmonic oscillator problem,

$$\ddot{\theta} = -\omega^2\theta , \tag{5.22}$$

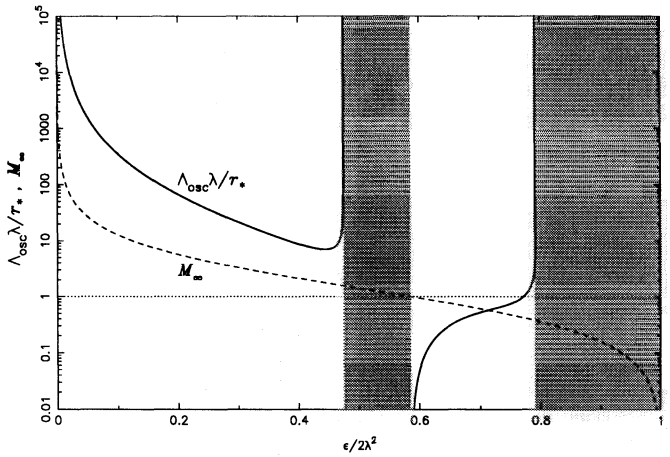

Fig. 3. Plot of the oscillation wavelength, $\Lambda_{\rm osc}$, normalized by $\lambda/r_\star$, as a function of the parameter $\epsilon/2\lambda^2$ (solid line). The corresponding asymptotic value of the Alfvén number is also plotted (dashed line). The shaded area corresponds to the region where the flow does not exhibit any oscillations. With a dotted line the limit $M = 1$ is shown, such that the right part of the plot ($\epsilon/2\lambda^2 > 0.58$) is out of interest, since there the solutions are asymptotically subAlfvénic

where the wavelength of the oscillations $\Lambda_{\rm osc.}$ is given by

$$\frac{4\pi^2 r_\star^2}{\Lambda_{\rm osc.}^2} = \omega^2 = 2\lambda^2 \left[\frac{2G_\infty^2}{(1-M_\infty^2)^2} \left(\frac{1-G_\infty^2}{1-M_\infty^2} + \frac{G_\infty^2}{M_\infty^2} \right) + \frac{M_\infty^4 - G_\infty^4}{2(1-M_\infty^2)^2(1-G_\infty^2)^2 M_\infty^4} \left(1 + \frac{G_\infty^4}{M_\infty^4}(1-2M_\infty^2) \right) \right]. \tag{5.23}$$

It is evident then that oscillations are a natural feature of the flow at long distances.

This result does not strongly depend on the model because as it is evident from Eq. (5.19) the only forces that act here are the centrifugal force combined with the magnetic forces (pressure + tension). Oscillations occur then because of the interplay of these two forces acting in opposite directions along the cylindrical radius distance ϖ. The only assumption is that pressure forces do not act perpendicular to the jet or they are negligible. This assumption is not unreasonable for the conditions along jets far from their source (Blandford & Payne 1982). Also, the choice we made for the α-dependence of the physical quantities can be seen as an expansion around the jet axis and this result seems to be of a rather general nature. It also leads to an interesting relation between the wavelength of the oscillations and the terminal values of the physical quantities of the flow.

The present model can be also compared to the analysis of Blandford & Payne (1982) and Pelletier & Pudritz (1992) where they have found one or multiple turning point(s) of the fieldlines. However, Blandford & Payne's self-similar solutions continue converging towards the polar axis contrary to the result found by Heyvaerts & Norman (1989) where they show that polytropic flows with $\gamma \neq 1$ should converge asymptotically to cylinders. While, the class of solutions presented by Pelletier & Pudritz (1992) may have some turning points but the authors did not perform a complete study along the axis to see how the cross section evolves. In the case of self-similar solutions, apparently the disagreement may arise because of the infinite current density along the polar axis which may act as an extra force bending the lines toward it. Here we have assumed right from the beginning that the polar axis is free of any current such that a final equilibrium is reached with pure cylindrical asymptotics in agreement with the conclusions of Heyvaerts & Norman (1989).

Those oscillations can be also compared to the self-similar model of Chan & Henriksen (1980). These authors found numerically oscillations in their self-similar solutions, although they assumed pressure confinement and included internal gas pressure which were considered as the protagonists in counterbalancing the pinching forces. It is then interesting to see that these oscillations may occur under other general assumptions without any help by the pressure, as indeed we have obtained here. In a forthcoming study it will be interesting to study the complementary case by introducing a pressure gradient across the fieldlines.

Now using Eq. (5.13, 5.14) the wavelength of the oscillations can be expressed in terms of the parameters of our model,

$$\Lambda_{\rm osc.}^2 = \frac{\pi^2 r_\star^2}{\lambda^2} \left(\frac{4\lambda^2}{\epsilon} - 1 \right) \left[1 - 2 \left(\frac{2\lambda^2}{\epsilon} - 1 \right)^2 \right]^2 \left(\frac{\epsilon}{4\lambda^2} \right) \frac{1}{1 + {\rm func}(2\lambda^2/\epsilon)}, \tag{5.24a}$$

where

$${\rm func}(x) = \frac{[2x(x-1)+1][x^2 - (x^2-1)^2(4x-1)]}{32x(2x-1)(x-1)^4[2x(x-2)+1]}. \tag{5.24b}$$

If the jet reaches high Alfvén numbers M, ϵ is small and in this limit func(x) is small compared to unity and can be neglected in Eq. (5.24). A parametric study can be easily performed then by using both, this analytical expression and the numerical results.

5.4. *Damping of the oscillations*

Another way of seeing the development of the oscillations and their damping (Fig. 2), is by writing the momentum balance across the streamlines in the following form,

$$\rho(\boldsymbol{V}_{\rm p}.\nabla)\boldsymbol{V}_{\rm p} - \frac{1}{4\pi}(\nabla \times \boldsymbol{B}_{\rm p}) \times \boldsymbol{B}_{\rm p} = \frac{B_\phi}{4\pi\varpi}\nabla(\varpi B_\phi) - \frac{\rho V_\phi^2}{\varpi}\nabla\varpi, \tag{5.25a}$$

where it is clearly seen from the RHS that the magnetic pinching force and the magnetic pressure gradient act towards the axis, while the centrifugal force of rotation acts away from the axis. The incomplete balance of those forces results in some central acceleration in the LHS. In other words, it gives rise to a curvature of the poloidal streamlines. In the final equilibrium where the jet is purely cylindrical, with no curvature of the poloidal

streamlines, the LHS vanishes and this equation reduces to Eq. (5.10). Keeping the dominant terms of this equation and using our notations, we find an equation for the second derivative of the cross section of the jet,

$$\frac{1}{R^2}\frac{\mathrm{d}^2 \ln G^2}{\mathrm{d}\ln R^2} = \frac{\lambda^2}{1-M^2}\left[4\left(\frac{1-G^2}{1-M^2}\right)^2 - \frac{2}{M^2}\left(\frac{M^2-G^2}{1-M^2}\right)^2\right], \qquad (5.25b)$$

where there is a one to one correspondance of the terms with the one in Eq. (5.25a). Eq. (5.25b) is simply another form of Eq. (5.19). The dependence on $1/R^2$ of the curvature of the fieldlines in the LHS explains the damping of the oscillations with increasing radius. This damping is then directly linked with the initial assumption that the Alfvén surfaces are spherical. Taking into account the curvature of the Alfvén surfaces thus leads to a spatially oscillating system and the oscillations are damping because the farther away from the source, the flatter the Alfvén surfaces are.

This result gives further insight in comparing with other self-similar studies. In the Blandford & Payne (1982) model, Alfvén surfaces are cones and the rotationnal axis is thus singular and no restoring force exists. In the Chan & Henriksen (1980) model, Alfvén surfaces are planes and oscillations must be of a different nature: as we have found, in the limit of flat Alfvén surfaces, the magnetic and centrifugal forces balance each other. However including strong pressure gradients lead to another type of oscillations where the restoring force is now due to the internal pressure. In their Appendix B, these authors write an equation similar to Eq. (5.25b) where the pinching term is balanced by the pressure term. This result may suggest then in the context of AGN the following scenario. On the small parsec scale knotty structure of the jet may be obtained through a process similar to the one presented here while oscillations on larger scales may be due to the Chan & Henriksen's (1980) process through the interaction with the external medium.

5.5. *Parametric dependence of the oscillations*

For fixed M_∞, which corresponds to a fixed ϵ/λ^2 through Eq. (5.13), the wavelength of the oscillations is inversely proportional to λ so that the oscillations almost disappear for small rotation (λ). Thus, in Fig. (3) $\Lambda_{\mathrm{osc.}}\lambda/r_\star$ and M_∞ are plotted as functions of $\epsilon/2\lambda^2$. An upper value of $\epsilon/2\lambda^2$ exists above which oscillations disappear. Also, numerical calculations show that the amplitude of these oscillations decreases as $\epsilon/2\lambda^2$ increase, or, M_∞ decreases. This may be seen in Fig. 2 where some solutions are plotted for fixed λ by varying ϵ. On the other hand, for $\epsilon \to 0^+$, $M_\infty \to \infty$ and the wavelength becomes infinite too as it can be shown from the analytical expression (5.24); the amplitude of the oscillations increases in this limit.

This result is to be compared with Blandford & Payne (1982) and Pelletier & Pudritz (1992) where the existence of a turning point in the solution exist when the solution reaches high values of the fast magnetosonic Mach number (FM number). Denoting with n the square of the FM number, they found that for values of n above some characteristic value n_t, solutions in the cold plasma approximation recollimate towards the axis. To make further comparison it is possible here to calculate the square of the fast magnetosonic Mach number as it is defined in the limit of the cold plasma approximation where asymptotically thermal effects are negligible. Following Blandford & Payne (1982), we denote it by n and give it here in the limit where cylindrical asymptotics are reached, $F \to 2$,

$$n \longrightarrow \frac{M_\infty^2}{1+\alpha G_\infty^2 \dfrac{G_\infty^2-1}{M_\infty^2-1}}, \qquad (5.26)$$

where it is clear that transAlfvénic solutions are fast magnetosonic at least around the axis. Exactly along the flow axis n reduces to M^2, as expected because the toroidal components vanish there (*cf.* Sakurai 1985).

The sound speed could also had been introduced explicitly right from the beginning, for example via the polytropic assumption, but this would not had changed qualitatively the above result. This is because at the fast magnetosonic speed we do not have a critical point in the present self-similar system. This is so, not only because we did not use the polytropic assumption. The main reason should be that taking into account both the Bernoulli and the transfield equations simultaneously in a consistent way, the resulting critical modes are strongly modified. A similar situation arises in isothermal self-similar solutions in cartesian geometry wherein the critical point does-not coincide with the sonic point, as illustrated in Tsinganos et al. (1993). This point was already present in Blandford & Payne's (1982) study where they had a possible critical point at $t = 1$, with t not the FM number but some critical speed ratio coming from the self similar assumption (see also beginning of Sect. 6). Moreover, none of the solutions they present are crossing this critical point which is always rejected to infinity. However, this does not prevent them from having two classes of solutions, one being trans-fast magnetosonic.

In Fig. (8), a plot of an oscillating solution is shown for $\lambda = 1.77$ and $\epsilon = 0.28$ in a two–dimensional plot of the real streamlines. In this case the wavelength is $\sim 1600 r_\star$ for a final $M_\infty \sim 30$ and a cylindrical radius of $4.68\ r_\star$. Note that according to Eq. (5.21) the amplitude of M is much smaller than that of F and also note that the scale has been compressed along the polar axis in the upper part of the plot. In reality oscillations are quite small in the geometry except for the very first one. As a numerical result, this example shows that the first oscillation occurs at about one wavelength from the base, that it is more dramatic here than in the following oscillations, while our prediction of the wavelength is underestimating the wavelength of the very first oscillations.

Since the density is proportional to the inverse of the Alfvén number, it is evident that these oscillations result in bumps of the density that might be related to the emission enhancements of the luminosity observed along several knotty jets, a point

however we shall discuss in more detail in another connection. The example chosen here emphasizes on purpose the first bump, although a more general exploration of the parameter set would show that the relative magnitude of the various oscillations depends strongly on the parameters, as it may be seen in Fig. 2.

6. Topological study of solutions in the subAlfvénic regime

After the previous section where we studied the asymptotics of the outflow by using the generalized Bernoulli integral, we turn now our attention to the region of the initial acceleration of the outflow, in the framework of our model.

As we discussed in Sect. 4, from the momentum equation one can immediately deduce the existence of critical points wherein the numerators and denominators of the equations become simultaneously equal to zero. With the assumption $\kappa = 0$ these critical points occur in the subAlfvénic part of the flow, similarly to what happens in the non rotating case studied in Paper II. Then, a three dimensional topology of the solutions can be drawn in the plane $[R, F, M^2]$, as in Paper II. In particular, in this section we shall examine how this topology of the solutions in the subAlfvénic region changes, as the rate of rotation increases. We shall see that there always exists a unique and physically interesting solution which is selected by an X-type critical point, similarly to the non-rotating case. This critical point is expected where the projection of the flow speed in the direction which preserves the self-similar symmetry of the system equals to a characteristic speed for MHD wave propagation. Thus, the critical transition occurs when

$$M^2 = 1 - \frac{\tan^2 \chi}{\tan^2 \theta}$$

where χ is the angle between B_r and the total component of the magnetic field in the θ, φ-plane. In other words $\tan^2 \chi = (B_\theta^2 + B_\varphi^2)/B_r^2$.

6.1. Parameters determining the solution

The parameters of our problem are the meridional distribution of the density, $\delta\nu^2$, the rotation rate λ, the meridional distribution of the Bernoulli energy, ϵ and the expansion factor at the Alfvén point, $F_\star$. Nevertheless, out of these four parameters only *two* are free, as we show in the following. So various ways of describing the parameters can be considered.

One way to proceed is to fix (i) the meridional distribution of the density, $\delta\nu^2$ and (ii) the rotation rate λ. Then, integrating the transfield equations (4.1b-f) upwind from the Alfvén point ($R = 1, M = 1$), we also need $F(R = 1) = F_\star$ in order to have a complete and unique solution that reaches low Alfvén numbers. Thus, $F_\star$ is determined by tuning the values of the slopes p and τ at the Alfvén point such that the solution goes through the X-type critical point and reaches low values for M at the base. Therefore, once $\delta\nu^2$ and λ are fixed, $F_\star$ is determined and the Bernoulli constant ϵ follows from Eq. (5.5a).

A *second* way to proceed is to start by fixing (i) the meridional distribution of the Bernoulli energy, ϵ, and (ii) the rotation

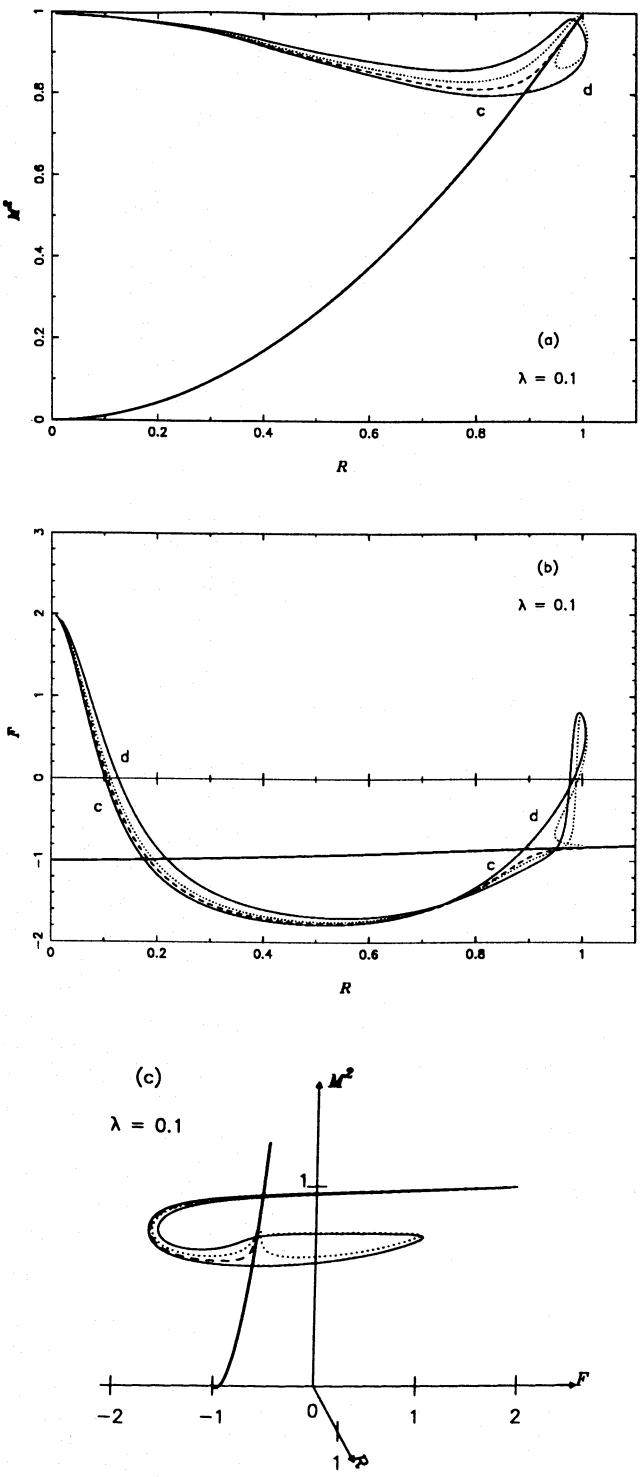

Fig. 4a–c. Topology of a slowly rotating system with $\epsilon = 0$ and $\lambda = 0.1$ in the $[R, M^2]$ plane, **a**, in the $[R, F]$ plane, **b**, and in the 3-D space $[R, F, M^2]$, **c**. The X-type critical point selects a unique solution that connects the Alfvén point to the origin (thick solid line). Non critical dashed branches (c) and dotted branches (d) are similar to the corresponding (c) and (d) of Paper II, except that the (d) branches cannot cross the Alfvén surface $M^2 = 1$ and are forced to turn back and converge to the **c** branches

rate λ. Then, we may deduce again the value of $F_\star$ by requiring that it satisfies the regularity condition (4.5) and the solution goes through the X-type critical point. Finally, $\delta\nu^2$ follows from Eqs. (5.5a) and (4.2) applied at $R = 1$,

$$\delta\nu^2 = \lambda^2[\tau^2(F_\star, \lambda) + 1] - 1 + \frac{F_\star^2}{4} - \epsilon\,. \tag{6.1}$$

A direct (albeit approximate) way of getting $\delta\nu^2$ solely in terms of ϵ and λ^2 is given in Eq. (6.6) below.

A *third* way to proceed is to start by fixing (i) the expansion function at the Alfvén point, $F_\star$ and (ii) the rotation rate λ. Then, according to the discussion given in Sect. 4, for given values of λ and $F_\star$, the slopes p and τ are naturally deduced from the regularity condition expressed by the cubics in Eqs. (4.4)-(4.5). If in addition we determine the value of the parameter $\delta\nu^2$ from the requirement that the solution reaches the base at R_o with vanishing Alfvén number (see Eq. (6.6) below), or equivalently it crosses the X-type critical point, the value of the Bernoulli constant ϵ is uniquely determined yielding the asymptotic outflow speed.

However, among those possibilities we shall choose to follow the second way in the rest of the section. Before proceeding with a detailed examination of the solution topologies in terms of the rotation parameter λ, we first estimate in the following the location of the "base" R_o of the wind in terms of the location of the characteristic Alfvén radius at $R = 1$.

6.2. *Approximate location of the stellar base of the outflow relatively to the Alfvén surface*

An estimation of the radius of the stellar source of the outflow can be obtained from the expression of the generalized Bernoulli integral alone. By denoting with R_o the radius at which the wind outflow starts ($R_o = r_o/r_\star$), we note that this radius determines the lower boundary of the region where the flow is slow and strongly magnetically dominated, i.e., $M \to M_o \approx 0$. Then, from the expression of ϵ (*cf.* Eq. 5.5a) in the limit of $M_o \to 0$, we obtain R_o in terms of G_o, in an expression which is evidently the generalisation of the corresponding Eq.(6.4) of Paper II,

$$R_o = \frac{\delta\nu^2}{2\lambda^2 - \epsilon - \lambda^2 G_o^2}\,. \tag{6.2}$$

If $\delta\nu^2 = 0$, then $R_o = 0$ and the stellar source of the outflow can be at the origin $r = 0$, as in Paper II. Similarly, if $R_o < 0$ the critical solution reaches $R = 0$. On the other hand, $R_o > 0$ only for $\delta > 0$ and $2\lambda^2 - \epsilon > \lambda^2 G_o^2$, or, $\delta < 0$ and $2\lambda^2 - \epsilon < \lambda^2 G_o^2$. Note that since $2\lambda^2 - \epsilon$ needs to be positive by the asymptotics of the wind (Eq. 5.14), the last case of $0 < 2\lambda^2 - \epsilon < \lambda^2 G_o^2$ and $\delta < 0$ gives unrealistically low values of the terminal Alfvén number because usually $G_o \ll 1$.

It is evident that the base of the outflow R_o is always at some interval, $R_o^{\min} < R_o < R_o^{\max}$, where,

$$R_o^{\min} = \frac{\delta\nu^2}{2\lambda^2 - \epsilon}\,, \qquad R_o^{\max} = \frac{\delta\nu^2}{\lambda^2 - \epsilon}\,. \tag{6.3}$$

The minimum value is obtained if the initial cross section of the jet is negligible compared to the cross section at the Alfvén surface, such that $G_o \approx 0$. This happens either because R_o is small and the stellar surface has a radius much smaller than the radius of the Alfvén surface, or because there is a large dead zone around the equator such that the last line connected to the base is rooted very close to the polar axis and $\varpi_o(\alpha_{\rm out}) \ll \varpi_a(\alpha_{\rm out})$. It is likely that jets where the material comes from the central star itself and not from a disc are in a situation not too far from this one in order to provide an efficient lever arm to extract angular momentum.

The maximum value occurs from the opposite assumption, namely that the fieldlines are already cylindrical from the stellar base, $G_o \approx 1$, a case rather extreme and therefore unlikely to happen. In this case the extraction of angular momentum from the star is minimal because the Alfvénic lever arm of the corotating region would be rather small.

Another way to estimate the value of G_o is the following. Since in the subAlfvénic domain and far away from the Alfvén distance, rotation is rather unimportant and the magnetic field rather strong, the geometry of the magnetic field lines there will be an intermediate one between the extremes of the dipolar geometry (magnetic effects dominant) and the radial geometry (outflow effects dominant, opening thus the fieldlines). The former holds in our model when $\delta\nu^2$ is small such that the initial thermal acceleration is not significant while the latter when $\delta\nu^2$ is rather large resulting in a large initial acceleration. Thus, we may write

$$f(R_o) \equiv f_o = \frac{1}{R_o^{1-t}}\,, \qquad F_o = -1 + t\,,$$
$$G_o \approx R_o^{1.5 - t/2}\,, \tag{6.4}$$

with $0 < t < 1$. When $t = 0$ we are in the case of the pure magnetospheric geometry without flows ($\delta\nu^2 \approx 0$) and $G_o = R_o^{1.5}$. On the other hand, when $t = 1$ we are in the case of pure hydrodynamic expansion ($\delta\nu^2 \gg 1$) and $G_o = R_o$. With $R_o \ll 1$ it follows that $G_o \ll 1$, unless λ is rather high. Thus, for finite $\delta\nu^2$ wherein the fieldlines initially expand radially ($t = 1$), an upper limit can be placed on R_o by substituting $G_o \approx R_o$ in Eq. (6.2)

$$\lambda^2 R_o^3 - (2\lambda^2 - \epsilon)R_o + \delta\nu^2 = 0\,. \tag{6.5}$$

For the examples shown in Figs. (4,5,6), this cubic gives for R_o: $R_o < 0$ when $\delta\nu^2 = -0.79$, $\epsilon = 0$ and $\lambda = 0.1$; $R_o \approx 0.35$ when $\delta\nu^2 = 0.69$, $\epsilon = 0$ and $\lambda = 1$; $R_o \approx 0.7$ when $\delta\nu^2 = 116$, $\epsilon = 0$ and $\lambda = 10$. These values are almost identical to those found by the detailed numerical integration, see Figs. (4,5,6).

Finally, if we want to get an approximate value of R_o without going through the numerical integration, we may use the approximation that the field lines are radial up to the corotation distance, such that $F_\star \approx 0$. Then, an approximate value for $\delta\nu^2$ is obtained by combining Eqs. (4.5) and (6.1)

$$\delta\nu^2 \approx 4\lambda^2 - 2\lambda\sqrt{2\lambda^2 + 1} - \epsilon\,. \tag{6.6}$$

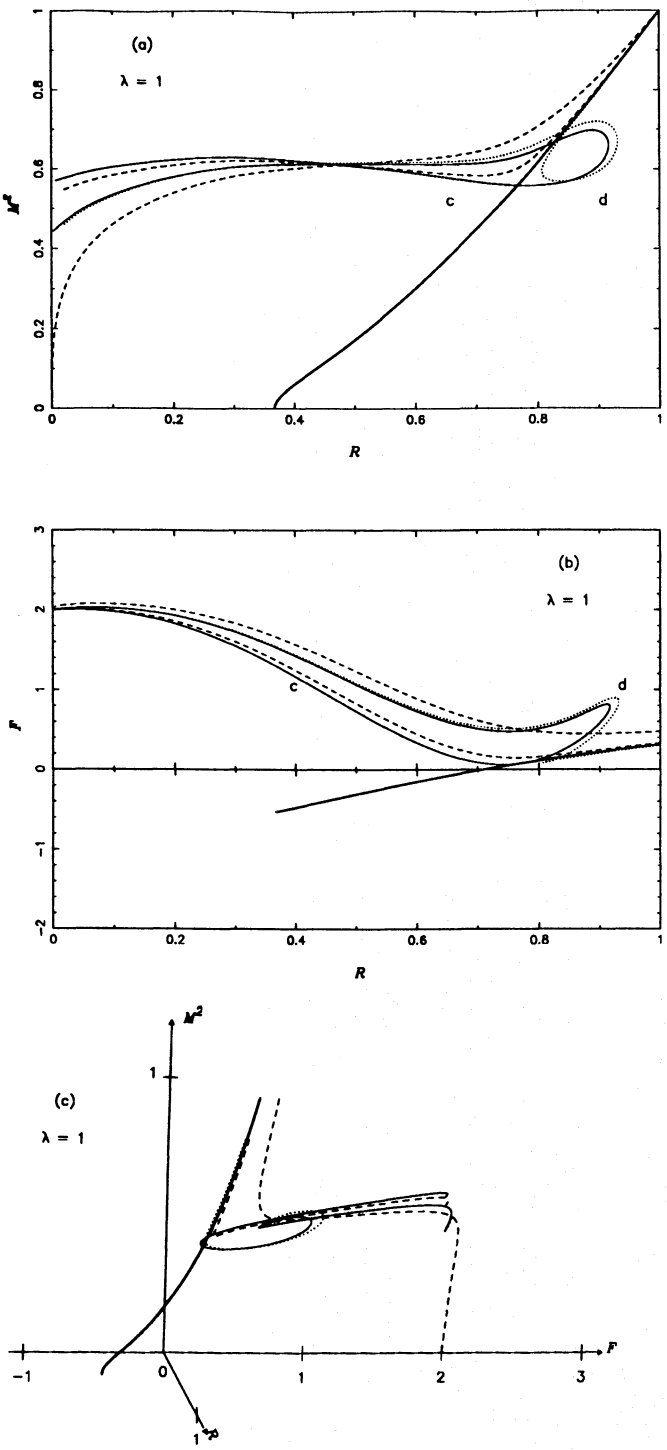

Fig. 5a–c. Topology of a system rotating at an intermediate rotational rate, for $\epsilon = 0$ and $\lambda = 1$, in the $[R, M^2]$ plane, **a**, in the $[R, F]$ plane, **b**, and in the 3-D space $[R, F, M^2]$, **c**. The critical solution (thick solid) is similarly selected by an X-type critical point. Dashed branches (c) and dotted branches (d) are similar to Fig. (4) except for the reversal in the $[R, F]$ plane where (c) branches are above (d) branches. We also plot a (c) branch that connects the origin $R = 0$ with some reasonable boundary conditions, e.g. $M = 0$, although it is not a critical one (see text for more details)

Comparing this value of $\delta\nu^2$ with the one used initially to obtain the cases shown in Figs. (4,5,6) we find that for $\epsilon = 0$ and $\delta\nu^2 \neq 0$, $\delta\nu^2 \approx 0.54$ when $\lambda = 1$ and $\delta\nu^2 = 116.45$ when $\lambda = 10$ which are very close to the actual values $\delta\nu^2 = 0.69$ and $\delta\nu^2 = 116$, respectively.

In the following we discuss how rotation modifies the topology by directly using our numerical results.

6.3. Topology of a slowly rotating system

It is reasonable to expect that for small rotational rates, the topology should resemble to the one found in Paper II. As an example, consider the topology of the solutions for $\lambda = 0.1$ and $\epsilon = 0$ which is plotted in the $[R, F]$ plane, the $[R, M^2]$ plane and the 3-D space, $[R, F, M^2]$, in Fig. (4). We see that the characteristic X-type critical point of the non rotating solutions is also present there, although the topology is slightly distorded by rotation. This critical point selects a unique solution that reaches the stellar base which in this case is at $R_o = 0$ because $\delta\nu^2 < 0$. The slope p of the critical line at $R = 1$ corresponds to the larger solution of the cubic (4.4) consistently with the fact that this is the only one that remains in the absence of rotation as explained in Sect. 4. In Fig. (1b) we mark with a bullet (•) the value of p at the Alfvén point, corresponding to the critical solution which passes through the X-type point.

In Fig. (4), we recover around the X-type point the topology of Paper II. In order to simplify the picture we did not draw the non critical lines that do not reach the Alfvén point, namely the lines labeled (a) and (b) in Paper II. Instead, we draw some non critical lines (c) and (d) and the second critical line. The main difference introduced by small values of the rotation is the change of those others branches around the X-type point. Branches (b) and (c) that were connected to $R = 0$, $F = -2$, are now forced by rotation to deviate and avoid this point, reaching finally $R = 0$ and $F = 2$. On the other hand, branches (a) and (d) that used to cross the plane $M = 1$ have first to turn over making a spiralling structure because rotation prevents them from becoming transAlfvénic; further on they just follow a similar path to branches (b) and (c) towards $R = 0$. Actually in the present case those noncritical lines reach $R = 0$ and $F = 2$ because δ is negative. They can reach also $F = \infty$ for other values of ϵ when δ is positive, as explained in Paper II. This same conclusion still holds further for somewhat larger values of λ.

Although the picture does not change drastically from the non rotating case, we already see that branches (c) and (d) are very similar except around the critical point. This means practically that it is very difficult to isolate numerically the X-type point by varying the shape of the lines at the Alfvén point and one may easely miss the interesting solution. The same conclusion holds again for stronger rotational rates.

6.4. Topology for intermediate rotational rates

For values of λ of the order of unity (grossly for $0.5 < \lambda < 2.5$) the X-type point remains but the surrounding topology is getting more and more affected by rotation. A typical such topology is

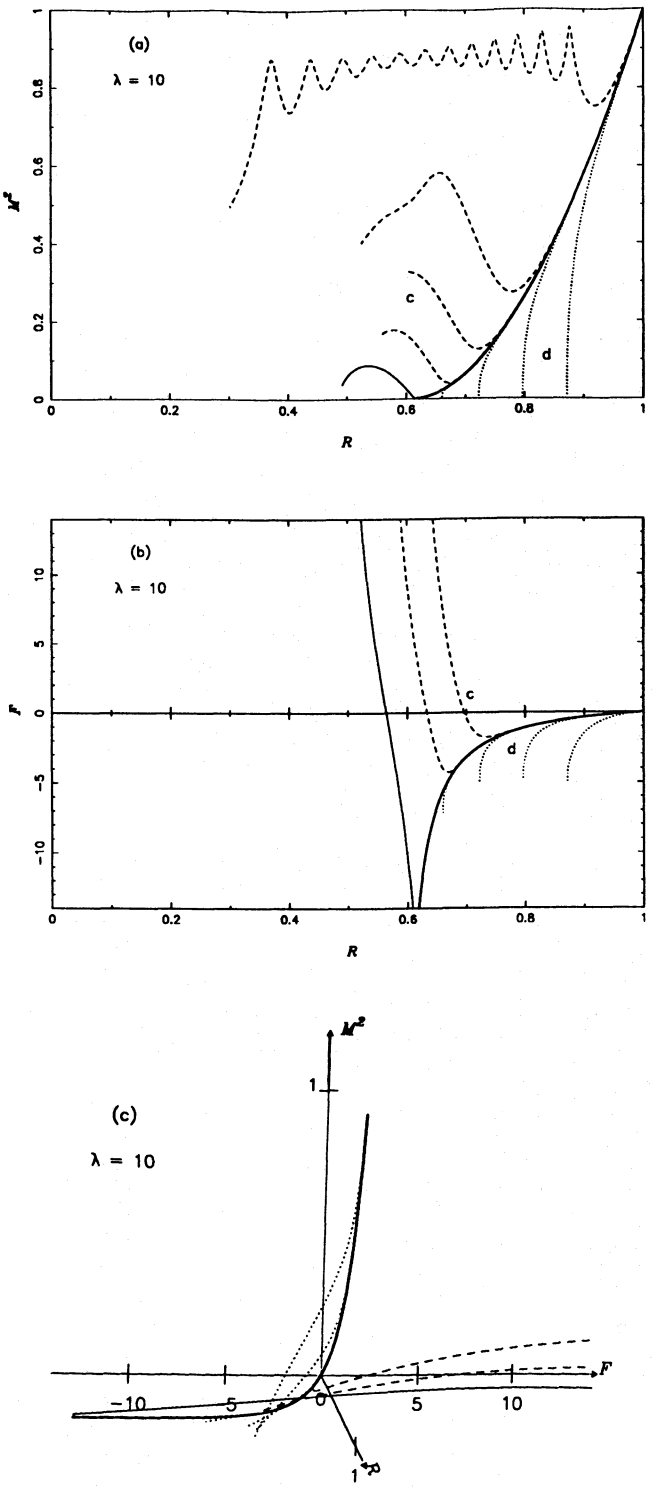

Fig. 6a–c. Topology of a fastly rotating system with $\epsilon = 0$ and $\lambda = 10$ in the $[R, M^2]$ plane, **a**, in the $[R, F]$ plane, **b**, and in the 3-D space $[R, F, M^2]$, **c**. The previous X-type critical point of Figs. 4 and 5 does not exist any longer and is replaced by an X-type critical point at $(R_o, F_o, M_o) = (R_{\min}, -\infty, 0)$. We also plotted the (c) and (d) branches with dashed and dotted lines, respectively. Note that any of the (d) branches may be physical but the critical solution (thick solid line) minimizes the input of energy

shown in Fig. (5), on the planes $[R, M^2]$ and $[R, F]$ and in the 3-D space $[R, F, M^2]$ with its two critical solid lines and non critical dotted/dashed lines labeled (c) and (d).

First, note that the X-type critical point for a given value of $\delta\nu^2$ is shifted to lower values of the Alfvén number M as λ increases. In Figs. (4,5,6) corresponding to the three representative values of λ, ϵ is kept fixed such that $\delta\nu^2$ increases when rotation increases; nevertheless it is not enough and the shifting up wind of the critical point is observed. It is obvious from Figs. (4a,5a,6a) that the X-type is farther and farther away from the Alfvén point. However $\lambda = 1$ is an intermediate case where the X-type point is still located at $M > 0$.

Second, branches (c) and (d) are now reversed at the Alfvén surface: branches (c) now correspond to values of $F_\star$ greater than the value on the critical branch while it is the contrary for (d). This feature shows up in Fig. 5b where around $R = 1$ dashed and dotted lines are obviously reversed as compared to Fig. 4b. This reversal compared to lower rotation may appear as a minor change that does not affect really the physics of the solution. Nevertheless it is responsible for complicating the topology and again should be treated with extreme caution in using numerical schemes.

We would like also to emphasize through this example that other critical branches may be sometimes obtained controlled by other critical points. Among the (c) branches that are displayed with dashed lines in Fig. 5, a unique solution goes to $[R, F, M^2] = [0, 2, 0]$. In Fig. (5c) this solution appears clearly as a dashed line connected to $F = 2$ at the origin. It apparently corresponds to a physical interesting solution although a more careful study shows that the strong widening of the jet before the Alfvén surface (corresponding to the jump from $F \sim 2$ to $F \sim 0.5$ makes a drop in the velocity quite unexpected. It corresponds also to a strong cooling in this region. The conclusion is that although the solution seems reasonnable at its boundaries (the source and the Alfvén surface) and it is a critical soltution in some sens, it is not necessarily a good solution. However, a further parametric study of these kind of solutions would be needed to exclude them completly. At present it is not completly excluded that a second class of solution that does not cross the classical X-type point may exist. The application of such solutions is however beyond the scope of this paper.

6.5. Topology for a rapidly rotating outflow

If we keep on increasing rotation, through an increasing of λ, the X-type point is shifted to negative values of M^2 which means that this critical point does not select a solution any longer. However, among the various solutions there is only one which reaches the minimum value for R, $R_{\min}$ discussed in Sect. 6.1 with corresponding values $M_o = 0$, and $F_0 = -\infty$. A more careful look into the momentum equation shows that this is an X-type critical point. An expansion around this X-type critical point can be performed, as

$$R = R_o(1 + \varepsilon)\,, \tag{6.7a}$$

and to second order it appears that the Alfvén number M (and not its square) is

$$M = 0 + O(\varepsilon^2)\,, \tag{6.7b}$$

while F diverges like

$$F = -\frac{1}{\varepsilon}\,, \tag{6.7c}$$

and G^2 approaches 0 like

$$G^2 = \frac{2\lambda^2 - \epsilon}{\lambda^2}\varepsilon\,. \tag{6.7d}$$

Considering now the critical solution, it suggests that for a fast rotating central object, the dead zone completely covers the stellar surface and the wind starts only from a very narrow polar region with an extremely high magnetic field. A similar result was found in Paper I, where the hydrodynamic and very fast rotating solutions were shown to be unphysical because all the lines were bending towards the equator except for the very polar one. The difference here is that the toroidal magnetic field rapidly grows up making possible to have some physical solutions through the pinching forces. However, in the source region lines are strongly bending towards the equator making a large dead zone around the star.

In fact, there is no absolute way to select a unique solution in the present case. The only criterion to have an acceptable solution is to require that it matches the stellar boundary conditions and in particular to have $M = 0$ there. As a matter of fact, any of the (d) branches shown in Fig. (6) could be used for that purpose. Note however, that the critical branch through this critical point, corresponds to the smaller base radius R_o and consequently to the bigger lever arm. Moreover, this solution has the smallest initial gradient for M, minimizing thus the input of initial energy.

6.6. How rotation controls the topology

Similarly to the superAlfvénic part, a global solution here is determined by the two parameters λ and ϵ. In particular, we have seen that R_o is determined by a combination of these two parameters which fix the value of $\delta\nu^2$ and the location of the X-type critical point that selects the physical solution; and this is just an extension of the analogous result obtained in Paper II without rotation. In Sect. 8 we shall discuss in more detail the parameter ϵ which gives asymptotically the amount of energy transfered into the toroidal components. Here however we emphasize that in the subAlfvénic regime λ emerges as the essential parameter for determining the location of the X-type critical point with respect to the Alfvén distance and subsequently determining the surrounding topology.

To illustrate this point note, through Eq. (3.19), that λ represents the angular momentum extracted per unit mass along each fieldline, in units of the Alfvén radius and velocity, or, it measures the initial angular speed of the footpoints of each streamline, in units of $V_\star/r_\star$. Thus, λ basically measures the rotational speed of the star that decreases with time as it evolves from a protostellar object to the final stages on the main sequence. In the subAlfvénic regime toroidal forces are important compared to other poloidal inertial forces (see Fig. 7 and Sect. 7 for a more detailed discussion on the dynamical regime in the solution), playing some important role in the topology. Farther away Poynting flux has been transfered to poloidal kinetic energy flux. This explains why $\epsilon/2\lambda^2$ is an important parameter. Conversely, it is not surprising that the topology in the subAlfvénic part is mainly controlled by the parameter λ while ϵ plays a minor role.

After this rather technical section, we shall now join the solution in both, the subAlfvénic and the superAlfvénic regimes to construct a complete solution from the source up to its asymptotics. However, we should keep in mind that the proper solution of the problem in the subAlfvénic part constitutes one of the most complicated parts of this study, with numerical work necessary to be done at some stage; and this may explain why several known studies have avoided to show a full solution from the source region to infinity. Yet, we believe that such a way of proceeding is absolutely essential to link consistently the observables at infinity together with the boundary conditions on the star.

7. Application to jets from YSO's

A full study of the applications of this model to various types of astrophysical jets or winds will be presented elsewhere. In this section we restrict ourselves to a preliminary application of the above analysis to jets from young stellar objects, keeping the discussion at a nondetailed level with our only goal to show the feasibility of such an undertaking. In particular, without going into the details of a specific object, we shall choose to outline our results for the case of the class of T Tauri stars and their associated jets.

7.1. Observational constraints

In the framework of the present model, the *dynamics* of a complete solution is determined by knowing the parameters ϵ and λ, while the *thermodynamics* of the flow by knowing the parameter ν and assuming a value for the asymptotic pressure Π_∞ (or temperature T_∞). Then, for each set of those four parameters an homologous class of solutions can be constructed. Furthermore, by specifying $r_\star$, $V_\star$ and $\rho_\star$, all physical quantities can be expressed in dimensional form which can be compared with observables, such as the terminal speed, rotational rate, etc. Altogether then, we need four parameters in order to determine the dynamics plus two for the thermodynamics.

A representative T Tauri star has a mass of the order of one solar mass (Malbet 1993), a radius of the order of a few solar radii, while its rotational speed at the equator is generally in the interval of 10 – 20 km/s (Bouvier 1986). Such a star usually has a well collimated jet which typically becomes visible at 100 AU (Pudritz 1990). This scale approximately determines

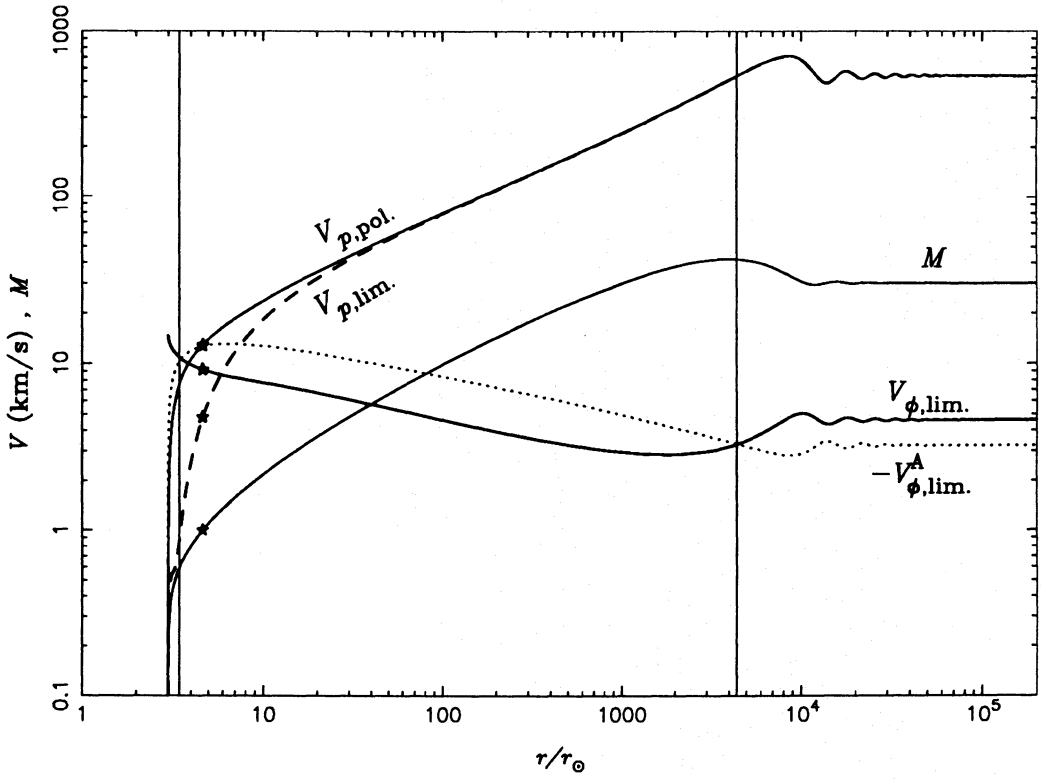

Fig. 7. Model I for a YSO, with $\epsilon = 0.28$, $\lambda = 1.77$, $r_\star = 4.65 r_\odot$, $V_\star = 13\,\mathrm{km/s}$, and various distributions of physical quantities with radius: the poloidal velocity along the axis of the jet $V_{p,\mathrm{pol}}$ (thick solid line), the poloidal velocity at the edge of the stellar jet and the disc wind $V_{p,\mathrm{lim}}$ (thick dashed line), the Alfvén number M (thin solid line), the toroidal velocity $V_{\varphi,\mathrm{lim}}$ (thick solid line) and the toroidal Alfvén velocity, $V^{\mathrm{A}}_{\varphi,\mathrm{lim.}} = B_{\varphi,\mathrm{lim}}/\sqrt{4\pi\rho}$ (dotted line), on the last line connected to the star. The Alfvén transition is denoted with a $\star$, while the left vertical thin line denotes the X-type critical point location. The right thin vertical line corresponds to the second crossing of $V^{\mathrm{A}}_{\varphi,\mathrm{lim.}}$ and $V_{\varphi,\mathrm{lim}}$.

the wavelength of the oscillations, *if* we assume that it corresponds to the location of the first oscillation/knot. Finally, the terminal speed is generally measured to be of several hundred km/s, although we may expect that the velocity along the jet axis is likely to be greater than the observed one (Pudritz 1990). Moreover, as proper motion of the knots is usually measured to be a few hundred kilometers, it is likely that we are still underestimating the terminal velocity of the gas itself flowing through the knots. In view of these constraints we choose the following set of observable variables of the problem :

$$\begin{aligned} &\mathcal{M} \approx 1\,M_\odot\,, \\ &r_o \approx 3\,r_\odot\,, \\ &\Omega \approx 7.\,10^{-6}\,\mathrm{rad/s} \quad \Longleftrightarrow \quad V_{\varphi o} \approx 15\,\mathrm{km/s}\,, \\ &\Lambda_{\mathrm{osc}} \approx 100\,\mathrm{AU}\,, \\ &V_\infty \approx 700\,\mathrm{km/s}\,. \end{aligned} \tag{7.1}$$

7.2. *Determination of model parameters from observational constraints*

Consider now the approximate determination of the parameters which completely define a solution. In order to do so, we shall use various analytical relations we have established in the previous sections. First, note from the definition of λ in Eq. (3.19a) that we have,

$$\Omega \approx \lambda \frac{V_\star}{r_\star}\,. \tag{7.2a}$$

Then making the assumption, which will be verified a posteriori, that the asymptotic Alfvén number is large, we know from Eq. (5.13) that the parameter $2\lambda^2/\epsilon$ is also expected to be large, so that we can use a simplified form of (5.24a) in this limit,

$$\Lambda_{\mathrm{osc}} \approx 2\frac{\pi r_\star}{\lambda}\left(\frac{2\lambda^2}{\epsilon}\right)^2\,, \tag{7.2b}$$

together with a simplified form of Eq. (5.16),

$$V_\infty \approx 2V_\star\left(\frac{2\lambda^2}{\epsilon}\right)\,. \tag{7.2c}$$

Eliminating $r_\star$, λ and ϵ from the three previous equations we get approximately the value of $V_\star$ in terms of the observable quantities

$$V_\star \approx \frac{V_\infty^2 \pi}{2\Lambda_{\mathrm{osc}}\Omega} \approx 15.7\,\mathrm{km/s}\,. \tag{7.3a}$$

Introducing this in Eq. (7.2a) gives for the ratio $k = r_\star/\lambda \approx 3.2\ r_\odot$ while using Eq. (7.2b) one gets $x = 2\lambda^2/\epsilon \approx 22.4$, which gives in turn from Eq. (7.2c) approximately the terminal Alfvén number, $M_\infty \approx 30$. Then we use the equations of Sect. 6, keeping in mind that $R_o = r_o/r_\star$. Thus, by combining Eqs. (6.5)–(6.6) together with the above results we get an implicit equation for λ where all the parameters are known, namely

$$\frac{r_o^3}{k^3}\frac{1}{\lambda^2} - 2\frac{r_o^3}{k^3}\left(1-\frac{1}{x}\right) + 4\lambda - 2\sqrt{2\lambda^2+1} - 2\frac{\lambda}{x} \approx 0\,. \quad (7.3b)$$

Solving this equation, we find a value of $\lambda \approx 1.77$ for the present set of observations, together with $\epsilon \approx 0.28$. As $r_\star$, r_o and $V_\star$ are known approximately, a value of ν of the order of $\nu \approx 22$ corresponds to a typical one solar mass star.

7.3. Model I for a jet from a YSO

Let us now fix the parameters of the problem and calculate the solution consistently. We actually need three dimensionless parameters, namely ϵ, λ and ν to define a solution, plus three reference values, i.e. $\mathcal{M}$, r_o and n_∞ (the terminal density along the jet axis), to translate all dynamical and thermodynamical quantities into physical units,

$$\begin{aligned} \epsilon &= 0.28\,,\\ \lambda &= 1.77\,,\\ \nu &= 22\,,\\ \mathcal{M} &= 1\,M_\odot\,,\\ n_\infty &= 10^3\ \mathrm{cm}^{-3}\,,\\ r_o &= 3\,r_\odot\,. \end{aligned} \quad (7.4a)$$

This set of parameters shall constitute what we call model I, in the following. Note, however, that we still have some flexibility in determining the last two parameters: for example, we could replace them by V_∞ and $\Lambda_{\rm osc}$, if observations were more precise on the values of those two parameters. Note, also that the choice of the terminal density is done *a posteriori* such as to explain the measured $10^4\ \mathrm{cm}^{-3}$ density in the surrounding emiting region, a point which we shall discuss in subsection 7.8 together with the thermodynamics. Note for a moment that the value $n_\infty = 10^3\ \mathrm{cm}^{-3}$ we have chosen, gives $\rho_\star = 1.7 \times 10^{-18}\,g\,\mathrm{cm}^{-3}$. Finally, the first three parameters define an homologous class of solutions where all members of this class differ only in the normalization.

Figures (7) and (8) display various physical quantities associated with this solution, which we shall review briefly. Note first that the solution topology is similar to the intermediate case we discussed in the previous section (see Fig. 5) with an X-type point in the subAlfvénic regime, located at $R_x = r_x/r_\star = 0.742$ that selects a unique critical solution going through the Alfvén point with $F_\star = 0.451$. Therefore, from Eq. (6.1) we find that $\delta\nu^2$ equals to 2.96 along this critical solution. Then, integrating upwind we find that the critical solution reaches a finite radius $R_o = r_o/r_\star = 0.645$ where $M = 0$. This radius practically defines the stellar base, since the magnetic field is dominant there and the velocity reaches zero. Note however, that the real stellar base may be identified just above R_o where the velocity is slightly positive. Fig. (7) shows however that practically this does not make any difference.

Thus, in this model I, the wind is blowing from $r_o = 3\,r_\odot$, passes through the X-type critical point at $r_x = 3.45 r_\odot$, corresponding to the left vertical line of Fig. (7), and accelerates up to the Alfvén surface located at $r_\star = 4.65\,r_\odot$ (noted with a $\star$ in Fig. 7). Using the definition of ν, the velocity of the wind at the Alfvén point is calculated to be $V_\star = 13$ km/s which is slightly lower than our initial guess. The wind continues accelerating until it collimates into a cylindrical shape after undergoing oscillations, see Fig. (8), reaching finally a terminal Alfvén number, $M_\infty = 30.2$. Also, we find the following values of the other physical quantities :

$$\begin{aligned} &\Omega = 7.07 \times 10^{-6}\ \mathrm{rad/s} \quad \Longleftrightarrow \quad V_{\varphi o} = 14.8\ \mathrm{km/s}\,,\\ &\Lambda_{\rm osc} = 44\ \mathrm{AU}\,,\\ &V_\infty = 543\ \mathrm{km/s}\,. \end{aligned} \quad (7.4b)$$

7.4. Dynamical evolution of flow

In Fig. (7), we plot the velocity along the pole, $V_{p,\rm pol.}$, the velocity along a streamline which is almost at the edge of the jet but is still connected to the star, $V_{p,\rm lim.}$, the azimuthal velocity at the limiting streamline, $V_{\varphi,\rm lim.}$, the Alfvén speed associated with $B_{\varphi,\rm lim.}$ — i.e. $V^{\rm A}_{\varphi,\rm lim.} = B_{\varphi,\rm lim.}/\sqrt{4\pi\rho}$ and finally the Alfvén number, M.

The polar outflow speed and the Alfvén number are increasing functions of the polar distance R and reach asymptotically maximum values once the jet becomes cylindrical, after some oscillations. For a nonpolar streamline which is away from the jet-axis, the initial velocity of the jet is lower, partly because δ is positive, but mainly because of the flaring of the streamlines, as found in Paper I. To see that we write the total poloidal velocity along a streamline as

$$V_p(R,\alpha) = V_\star \frac{M^2}{G^2}\sqrt{\frac{1+\left(\dfrac{F^2}{4}-1\right)\dfrac{G^2}{R^2}\alpha}{1+\delta\alpha}}\,. \quad (7.5)$$

Along the pole $\alpha = 0$, while for a non polar streamline close to the equator, we have $\alpha \lesssim 1$ and $F^2 < 4$ because of the streamline geometry [see Fig. (8)]. It obviously introduces in the numerator a decreasing factor as we move from the pole to the equator.

The terminal speed is also reduced due to the positive value of δ as we move farther away from the jet to the disc-wind region. As $F \sim 2$ in the asymptotic region, we see from Eq. (7.5) that the anisotropy from line to line is mainly due to the effect of δ at the denominator. This feature does not appear clearly in Fig. (7) because δ is too small. Differences between the polar streamline and the streamline at the edge of the stellar jet are negligible.

Figure (7) shows the various stages of the acceleration in the wind. There are mainly three distinguishable zones, separated

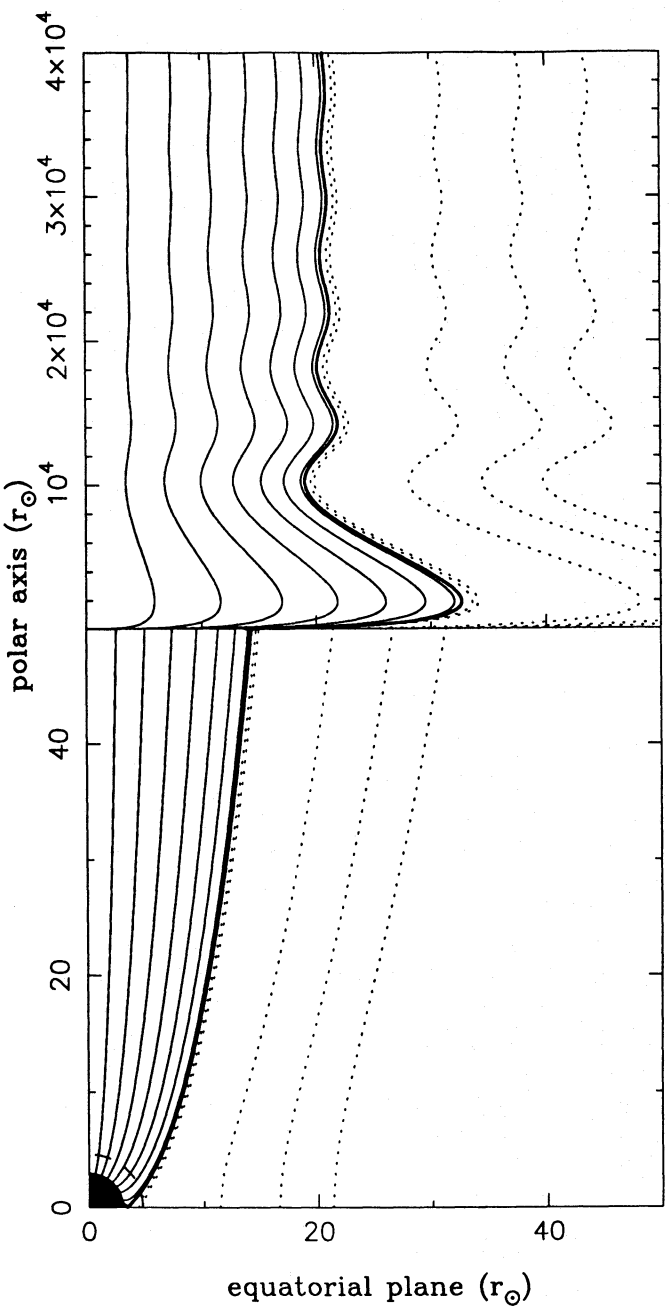

Fig. 8. Plot of the shape of the streamlines in the poloidal plane of model I with two different scales along the polar axis. The stellar wind (thin solid) is separated from the disc wind (dotted) by the last line connected to the star in thick solid line. Below, we plot the initial accelerating and collimating region near the star with the same scale on both axes. The Alfvén surface is drawn with a dashed line. On top, oscillations are shown with the terminal cylindrical shape and the polar axis scale is reduced on purpose

in Fig. (7) with two thin vertical solid lines. They correspond to the *three* different acceleration regimes in the wind as follows.

Up to the X-type point the wind is undergoing an initial *thermal* acceleration corresponding to a strongly heated region (for more details see paragraph 7.8 of this section). At this stage the toroidal components do not play any significant role in the initial acceleration of the wind. The toroidal speed V_φ which carries the initial angular velocity of the foot points, decreases while the toroidal Alfvén speed $V_\varphi^{\rm A}$ increases rather sharply. The X-type critical point corresponds to the transition region where both velocities are approximately equal. This gives some new insight to the meaning of this critical point. It corresponds to the point where toroidal pinching forces start getting dominant over the centrifugal forces and where the wind switches from a thermally driven to a magnetically driven one.

From the X-type critical point downstream, both toroidal components decrease, since there is some energy transfer from the centrifugal component and the Poynting flux to the poloidal component. Thus, the poloidal velocity undergoes a much smoother acceleration as a signature of magnetic effects. In this region, the pinching forces dominate over the centrifugal forces. Moreover, as the heating source gradually vanishes, all the thermal forces vanish too (see Fig. (9) and discussion hereafter 7.8). The net result is that the lines focalize toward the axis.

This inward converging of the lines spins up the wind again and we reach a new stage where both V_φ and $V_\varphi^{\rm A}$ are equal (right vertical thin line). At this point the interplay of the toroidal components creates oscillations that we shall explain later together with the corresponding streamline shape in this regime.

7.5. Streamline shape

In Fig. (8), the poloidal fieldlines are plotted and they show again three different regimes corresponding to the three previous dynamical regimes.

Initially, the streamlines show a strong flaring. This flaring is due to the large heating and corresponding large pressure gradient in the radial direction $\mathrm{d}P/\mathrm{d}R$, which has also a strong component in the ϖ-direction, $\mathrm{d}P/\mathrm{d}\varpi$, repelling thus the streamlines away from the flow axis. Later, as the heating and subsequently the pressure gradient $\mathrm{d}P/\mathrm{d}\varpi$ sharply decrease [see Fig. (9c)], the streamlines return to their radial shape.

However, now the azimuthal magnetic field has built its strength enough to start pushing the streamlines towards the flow axis and collimation starts. This corresponds to the second dynamical regime from a few $r_\odot$ up to approximately 4000 $r_\odot$.

The third dynamical regime is the one with the oscillations where the toroidal forces dominate in the transverse force balance. It approximately starts when both toroidal velocity and toroidal Alfvén speed are equal. At this point, lines are converging, increasing thus the toroidal velocity. However, the existence of centrifugal forces prevents the flow from focalizing completely at the pole. The jet undergoes oscillations due to the interplay of the centrifugal force, the magnetic tension and the magnetic pressure gradient. Asymptotically, the difference between the two speeds in Fig. (7) reflects the existence of a finite magnetic pressure gradient at equilibrium. Each minimum (maximum) in the jet radius [see Fig. (8)], thus corresponds to a maximum (minimum) in the azimuthal velocity and to a minimum (maximum) in the azimuthal Alfvén speed. At each

extremum there is a restoring force which brings the jet toward equilibrium. In between, the toroidal velocities reach their asymptotic values, but the curvature of the streamlines is associated with some extra transverse forces making thus the system to oscillate around its asymptotic position. These oscillations exist because we have taken into account the curvature of the Alfvén surfaces with respect to R. As we go farther away in the jet this curvature decreases, thus resulting in a damping of the oscillations. Finally, the jet reaches equilibrium in a cylindrical configuration as explained in Sect. 5.

Between the top and the bottom plots, the apparent kink in the lines is an artifact of the plot and it is due to the different scale. As we already noted in Sect. 5, the first throat in the jet is more dramatic than the following oscillations and is the more likely to be where the jet starts becoming visible. However, it must be emphasized that in order to "resolve" the jet horizontaly, the equatorial axis has been much enlarged as compared to the polar axis making the effect of oscillations more pronounced than it really is. The thick line indicates the very last streamline connected to the star and actually separates the stellar wind component of the jet from the disc wind component. Lines that are not connected to the star (with dots in Fig. 8) may then naturally correspond to lines rooted in the disc itself.

The wavelength of the oscillations is smaller by more than a factor of two than our initial guess because of the approximate form of Eq. (7.2b) and we only kept this formula in order to make some starting guess of the actual value. Note the following regarding these oscillations. *First*, the first throat [cf. Fig. (8)] is located around $R = 2100$ corresponding to

$$\Lambda_{\text{first throat}} = 58\,\text{AU}\,. \tag{7.6}$$

Second, the wavelength is rather sensitive to the terminal Alfvén number and increases rapidly as M increases slightly (Fig. 3). *Finally*, note that available observations are not so precise as to take our initial guess strictly. Here, the first throat corresponds to the point where the jet becomes visible; and this is not known better than a factor of 2. In Fig. (10), we present another solution where the wavelength is much larger, just to show that by shifting the parameters it is possible to adjust more precisely the observations.

7.6. Mass loss rate

From Fig. (8) and the discussion of the previous subsection, it is evident that there exist two components in the jet, one being of stellar origin and the other one produced by the disc. However, they do not have the same contribution to the total mass loss rate of the system, as we shall see.

From Eqs. (3.10) and (3.7a), it is possible to calculate the mass loss rate along a flux tube of asymptotical cylindrical radius ϖ_∞,

$$\dot{M}(\varpi_\infty) = \pi r_\star^2 \rho_\star V_\star \frac{2}{3\delta}\left[(1+\delta\frac{\varpi_\infty^2}{r_\star^2 G_\infty^2})^{3/2} - 1\right]. \tag{7.7}$$

Using the values of model I, we find that the stellar component of the jet carries approximately $5 \times 10^{-15}\ M_\odot$/yr, while a jet extending to only 42 AU can account for a mass loss rate of $10^{-8}\ M_\odot$/yr as observed. Thus, the stellar component in Model I does not contribute significantly to the total mass loss rate but it is instead the disc-wind which is mainly responsible for the mass loss rate, a fact in agreement with recent observations which relate the wind mass loss rate to the accretion mass loss rate (Edwards et al. 1989; Cabrit et al. 1990). Also, it is still the inner part of the disc that is responsible for the total mass loss rate within our model. And, an even inner part of the disk is responsible for the total mass loss rate if we allow a transerve pressure gradient ($\kappa \neq 0$) as we shall explain at the end of this section.

7.7. Poloidal electric current

Our modelling is rather general along the rotational axis and should therefore reproduce some features of other models. In particular, it is interesting to show that the flow along the axis can be modelled in a consistent way, avoiding a complete focusing of the lines on the pole, as is the case for example in several other disc-wind models (Sakurai 1985, 1987; Blandford & Payne 1982; Pelletier & Pudritz 1992), because the question of the current density along the axis has been correctly addressed. As we have shown just above, the present model may account for the inner current-carrying part of the jet composed of the proper stellar wind and the inner core of the disc wind necessary to collimate the jet. Then, the solution can be eventually matched outside to a wind that does not carry any poloidal current as suggested by Pelletier & Pudritz (1992).

Actually, the dependence of all toroidal components across the jet can be deduced easely from Eqs. (5.7) and (5.8) in the asymptotic regime. There, we have that

$$\begin{aligned} &B_{\varphi\infty}(\varpi) \propto \varpi\,,\\ &V_{\varphi\infty}(\varpi) \propto \text{const.}\,,\\ &j_{\text{pol.}\infty}(\varpi) \propto \text{const.}\,,\\ &I_{\text{pol.}\infty}(\varpi) \propto \varpi^2\,, \end{aligned} \tag{7.8a}$$

where $j_{\text{pol.}\infty}$ and $I_{\text{pol.}\infty}$ are the current density and the total poloidal current in the jet. These asymptotic dependences can be compared with those in the self similar model of Chan & Henriksen (1980), although here the increase of the mass flux (and therefore of the density) with the cylindrical radius allows the rotational speed to reach a constant value and not to diverge as in their model. More precisely, the poloidal current enclosed in a flux tube of terminal cylindrical radius ϖ_∞ is given by (3.17)

$$I_{\text{pol.}\infty} = \lambda \frac{cB_\star}{2r_\star}\frac{\varpi_\infty^2}{G_\infty^2}\frac{1-G_\infty^2}{1-M_\infty^2}\,, \tag{7.8b}$$

such that this model requires a rather small current flowing into the jet. Taking the values of model I, we find that the inner part of the jet carries the current,

$$I_{\text{pol.}\infty} = 1.81 \times 10^7\ \frac{\varpi_\infty^2}{r_\odot^2}\ \text{A}\,. \tag{7.8c}$$

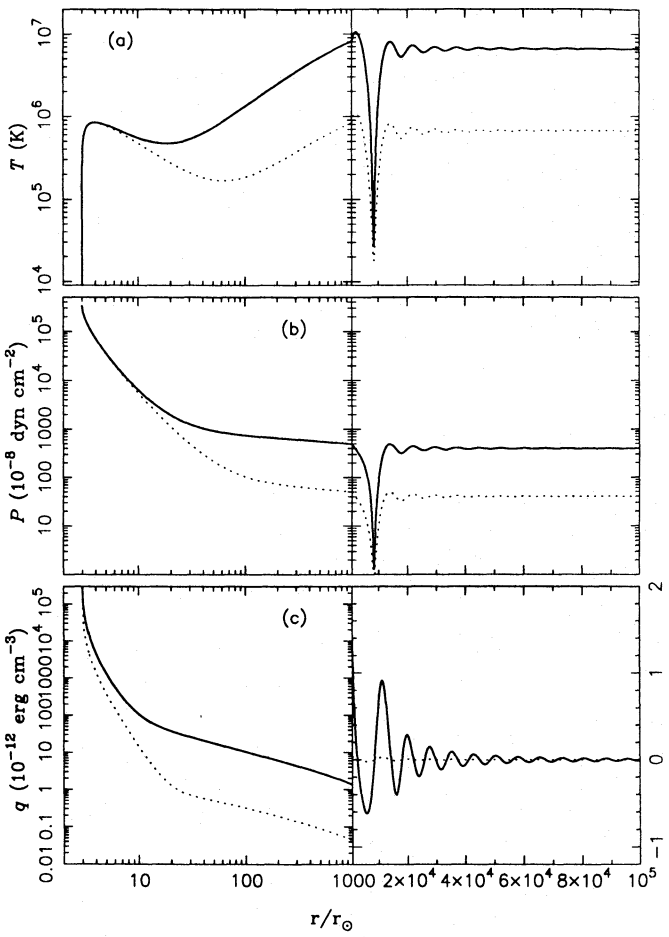

Fig. 9a–c. Plot of the polar temperature, pressure and heating profiles in **a**, **b** and **c** for model I (solid line). Parameters are given in Fig. 8, together with $\rho_\star/m_p = 10^6$ cm^{-3}. In addition we have plotted a second solution (dotted line) where velocities have been reduced by a factor of $\sqrt{10}$ as compared to model I, but everything else is kept identical (i.e. λ, ϵ, $r_\star$, $\rho_\star$ and $\mathscr{M}$ are as in model I but $V_\star$ is changed to $V_\star/\sqrt{10}$)

A total current of about 10^{10} A is flowing within 3 AU in a core jet and this would be enough to support a surrounding current-free flow as suggested by Pelletier & Pudritz (1992).

7.8. Thermodynamics

Let us turn now our attention to the thermodynamical features of the solution corresponding to model I and illustrated in Figs. (7) and (8). In the following Fig. (9a) we plot the temperature, in (9b) the pressure and in (9c) the heating rate per unit volume, along the rotation axis of the flow, with the curves corresponding to model I displayed with a solid line. At the same plots we have also drawn with dotted lines the curves corresponding to another solution where all parameters are kept identical to model I except that the velocities have been divided by a factor of $\sqrt{10}$ (the terminal velocity is now 220 km/s and the equatorial velocity of the star is 4.96 km/s) and $\nu = 70$.

As we already mention in Paper I, the pressure and consequently the temperature, can be adjusted by renormalization as long as $\kappa = 0$, because the pressure just enters through its gradient in Eq. (4.1a). However, there exists a lower limit here, in order for the pressure to remain positive everywhere. Thus, we have chosen arbitrarily some asymptotic values for the pressure in Fig. (9b) which are close to the lower allowed value. Hence the pressure almost goes to zero in the very first oscillation where it reaches its minimum value. For model I wherein $\nu = 22$, we choose $T_\infty = 6.5 \times 10^6$ K (solid) while for the lower velocity model with $\nu = 70$, $T_\infty = 6.7 \times 10^5$ K (dashed). Globally we see that by reducing the velocity, it is easy to reduce within the model the terminal temperature and pressure although their initial values are not affected, since the escape speed does not change.

In Figs. (9b,c,d), for the temperature, pressure and volumetric heating rate profiles along the polar axis we may distinguish several regimes in the radial dependence of those thermodynamic variables.

- *First*, we have a high heating rate which builds up a large pressure gradient that helps the wind to escape from the gravitational well of the star. Thus, most of the heating is concentrated near the star and drops fast, consistently with the idea that most of the heating processes are coming from the star or its surrounding disc and are damped with the distance. With the flow expanding radially such that the density drops only like R^{-2}, a sharp temperature increase results then as in the chromospheric transition region (Papers I and II).
- *Second*, subsequently the heating and therefore the pressure gradient level off, the pressure decreases slower and the temperature starts to decrease too, also as found in the radial case of Papers I and II.
- *Third*, when the geometry deviates from radial and collimation starts, the pressure drops even much slower, essentially balancing the gravitational well only since the inertial terms in this regime are small. This is the case just before oscillations appear because F is close to 2 and the inertial terms in Eq. (4.1a) are proportional to $M^2(F-2)/R$. In other words, the pressure goes almost to a constant value once the deviations from radiality are strong enough and the gravitational effects become small. Such a combination could not exist in the previous noncollimated solutions as the ones found in Papers I and II: in an asymptotically radial wind the pressure keeps on decreasing like R^{-3} all the way long, to zero at infinity. Thus, now the pressure rapidly becomes constant forming a plateau that corresponds to the asymptotic value reached after collimation is achieved. The density is still droping fast and consequently the temperature rises to higher values. This is the case just before oscillations appear.
- *Fourth*, once the flow starts undergoing oscillations, the pressure in the jet undergoes small oscillations too (as compared to the initial pressure gradient needed to push the wind out of the gravitational potential) because of the kinematic forces that appear again in Eq. (4.1a). In particular, as $F > 2$ in Eq. (4.1a) the pressure needs to drop faster in order to balance the term proportional to $F-2$ in Eq. (4.1a). Combining this with the result that the density increases as the jet ma-

terial moves towards the throat, the temperature decreases sharply. When the lines start bending strongly towards the pole, more than cylindrical (between 1000 and 10000 $r_\odot$ in Fig. 8), the total heating becomes negative as it can be verified in Fig. (9) independently of the velocity. This net cooling effect is responsible for the drop of the temperature shown in Fig. (9a). It actually suggests that the effect of focusing by the pinching magnetic forces can be associated with radiative losses. However, the total cooling in this region is unlikely to be only radiative, since a larger or smaller part of it may be of magnetic origin (Alfvén waves) and be reprocessed in the next opening of the fieldlines where heating takes place once more.

- *Finally*, after the oscillations decay the pressure, temperature and density relax to their constant values while the heating drops to zero. Note that the density profile is the inverse of the Alfvén number distribution given in Fig. (7).

The high temperatures are associated with low density regions so that it is quite unlikely that those regions will have any radiative emission. Moreover, δ is positive which means that the density increases outwards and that the temperature decreases across the section of the jet. Thus, it is quite likely that the outer regions of the jet have the main contribution to the observed portion. The transverse drop of the temperature is given by

$$\frac{T(\varpi)}{T_{\rm pol.}} = \frac{1}{1+\delta\dfrac{\varpi^2}{G^2 r_\star^2}} \,. \tag{7.9}$$

In model I, for example and in the asymptotical region the temperature drops by a factor of 10 within 5 AU and by a factor of 100 within 16 AU across the jet. So, relatively close to the jet axis the temperature drops to a few 10^4 K, as implied from the observation of the optical jets. This may be reduced even more if tranverse gradient pressure were allowed as we shall explain later on. Another way to reduce globally the temperature is to reduce the velocity, as it is shown with the dotted curves in Fig. (9a). Although we did not perform any calculation of the luminosity, the inner hot core is likely to have no detectable counterpart (visible or X-ray emission), the same way the hot corona of the sun after a few solar radii is undectectable. However, in the throat of the jet itself, very low temperatures can be achieved, even close to the polar axis. There the temperature can reach very low values down to 10^4 K and beeing associated with some enhancement of the density there, it would favor in addition to a spatially continuous emission from the outer part of the jet, some brighter knot emission. Thus, the very first point of focusing which we called the first throat, may be a good candidate for the formation of a visible knot and it may be also the only one in the frame of the present model. As proper motion is usually measured within those knots, it could be that the series of knots usually observed are resulting from the time-dependent evolution of the jet which is of course out of the aim of the present modelization.

Altogether, we have found that the present model shows some interesting properties in describing the thermodynamics of jets, although it does not contain explicitly an energy equation. It also displays some of the limitations of the model, mainly because of the absence of a tranverse pressure gradient, an assumption we abandon in a companion study. Such a refinement of our approach may improve the situation, for example by reducing the temperature everywhere in the jet, as we shall explain in a following subsection. However, we note that such effects of the thermodynamics are of second order as far as the dynamics of the flow in its asymptotics are concerned (which is anyway close to the cold plasma description). In closing we mention that in this subsection we have restricted our attention to the thermodynamics of collimated flows. The thermodynamics of noncollimated which become asymptotically radial on the other hand, has been already discussed in Papers I and II, as well as in Tsinganos & Trussoni (1991).

7.9. Model II for a jet from a YSO

An important feature of the previous solution is that the Alfvén surface turns out to be rather close to the stellar base, with a corresponding lever arm $\varpi_a = 1.5\,\varpi_o$, as compared for example to the solar case. We note that this result has emerged naturally from our parameters chosen to fit the observations. Usually it is convenient to assume that the Alfvén surface is rather far from the star in order to decouple the thermodynamics and use the cold plasma approximation. Note however that also in other self-similar solutions (Blandford & Payne 1982) the Alfvén surfaces are converging towards the center. There is even a singularity in this case as all Alfvén iso-contours cross the origin. By comparison, in the model of Sakurai (1987) it is suggested that the Alfvén surface could be far from the disc but it changes of topology near the star and gets closer. The lever arm of the disc wind would then be enhanced and responsible for the angular momentum loss. As it has been shown by Pudritz & Norman (1986), the stellar wind cannot do it by itself and this seems to be confirmed here. Nevertheless, the central part of the jet, modelled here, could be an important component to explain the overall structure of the flow as we have just shown. Finally, X-ray observations suggest that the acceleration region is very close to the star within a few stellar radii, comforting the idea that the Alfvén surface would be closer than expected (Natta 1990).

However, to show that the model can reproduce a jet with a more extended lever arm, we plot in Fig. (10) the poloidal two dimensional configuration of the streamlines. The thick line again separates the stellar wind from the disc wind. The set of parameters used for this solution, called model II, is

$$\begin{aligned} \epsilon &= 0.07\,, \\ \lambda &= 0.8\,, \\ \nu &= 4.5\,, \\ \mathscr{M} &= 1\,M_\odot\,, \\ r_o &= 3\,r_\odot\,. \end{aligned} \tag{7.10a}$$

The Alfvén surface is now found to be at $r_\star = 7.8\,r_o = 23.4\,r_\odot$, with an Alfvén speed $V_\star = 28.4\,\mathrm{km/s}$ and the X-type critical

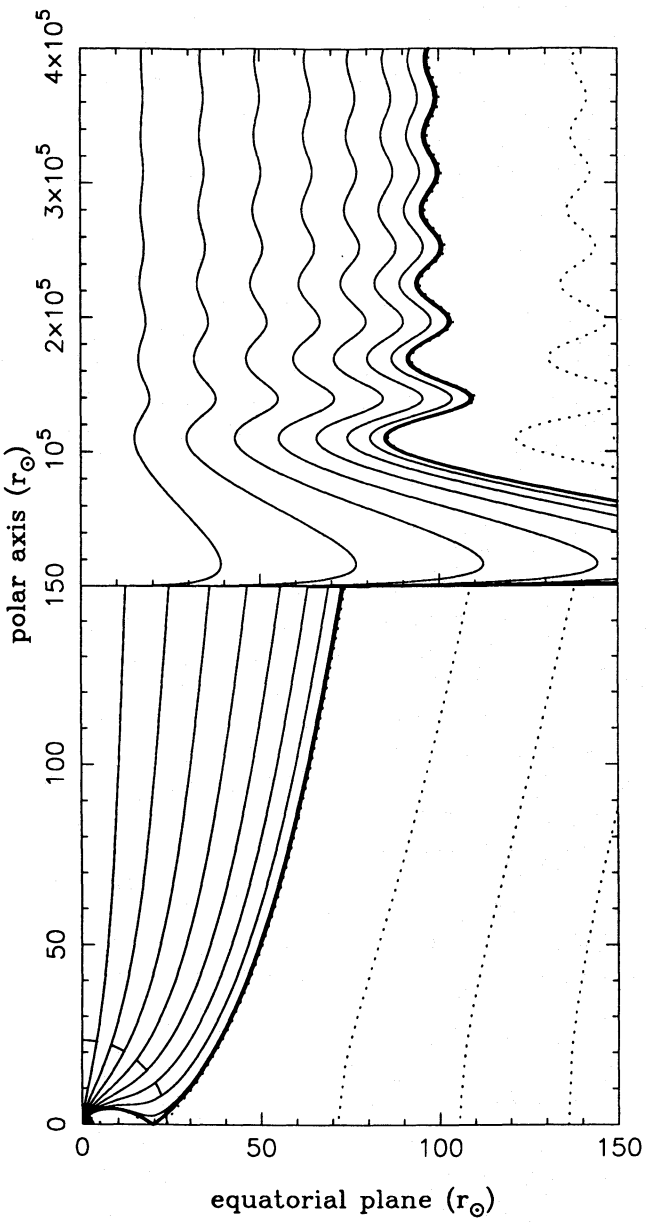

Fig. 10. Similar plot as Fig. (8) for model II with $\epsilon = 0.07$, $\lambda = 0.8$. The dead zone is much bigger and the Alfvén surface farther away from the star. On top, the wavelength of the oscillations is much larger than in model I

point is located at $r_x = 6.13\, r_o = 18.4\, r_\odot$. As the dead zone is important, the ratio of the magnetic lever arm to the stellar lever arm is even higher than the ratio of the Alfvén radius to the stellar radius. We find altogether

$$\begin{aligned} \varpi_a &= 14\,\varpi_o\,, \\ \Omega &= 1.4\,10^{-6}\,\mathrm{rad/s} \quad \Longleftrightarrow \quad V_{\varphi o} = 2.9\,\mathrm{km/s}\,, \\ \Lambda_{\rm osc} &= 320\,\mathrm{AU}\,, \\ \Lambda_{\rm first\ throat} &= 642\,\mathrm{AU}\,, \\ V_\infty &= 950\,\mathrm{km/s} \\ M_\infty &= 24\,, \end{aligned} \tag{7.10b}$$

Note that the wavelength here, is much larger than in the previous model and corresponds more or less to the spacing of the HH objects in HH 33–34 (Reipurth 1990) which is of the order of 0.004 pc = 825 AU. For such an object, the velocity of the gas inside the jet should definitely be larger than the proper motions of the knots in the jet; such a study needs to be carried in the framework of a time dependent model.

If a specific object is to be modelled, of course the present scheme can be used iteratively until convergence is reached between the observations and the final solution. Such a detailed modelling is however outside of the scope of the present paper. We have simply shown here that our study is capable to describe such a phenomenon and our model is rather flexible for the various parameters of the observations.

8. The transition from jets to winds

In Sect. 6 the boundary conditions at the source of the outflow were connected to the conditions at the Alfvén surface while in Sect. 5 we linked the conditions at the Alfvén surface to those at the asymptotics. In Sect. 7 we have illustrated the collimated solutions by applying them to jets from T-Tauri stars. In this section we shall try to characterize quantitatively in the frame of our modelling how collimation takes place and to link it with the boundary conditions at infinity and at the stellar surface. Our aim is then to give a general criterion and to explain why we obtain those two different classes of solutions.

8.1. A criterion for collimation

From the previous sections, it appears that giving the two parameters ϵ and λ in the frame of our modelling completely determines the geometry of the solution. In the following we discuss the physical content of this key combination of the two parameters, $\epsilon/2\lambda^2$. Thus, first note that

$$\begin{aligned} \frac{\epsilon}{2\lambda^2} &= \frac{\rho(R,\alpha)F(\alpha) - \rho(R,\mathrm{pole})F(\mathrm{pole})}{\rho(R,\alpha)\Omega(\alpha)L(\alpha)} \\ &= \frac{\Delta(\rho F)}{\rho\Omega L}\,. \end{aligned} \tag{8.1}$$

Evidently this parameter measures the excess of the volumetric total energy along a given field line, as compared to that energy along the pole, normalized to the corresponding volumetric magnetic rotator energy, $\rho\Omega L$.

Expressing $\epsilon/2\lambda^2$ in terms of the conditions at the source boundary r_o where the cylindrical radius is $\varpi_o(\alpha)$, the escape speed $V_{esc,o}$, the polar density $\rho_o(\mathrm{pole})$ and the density at any other streamline $\rho_o(\alpha)$, we find from Eq. (6.2) that for the case $\delta \neq 0$,

$$\frac{\epsilon}{2\lambda^2} = 1 - \left[\frac{E_{\rm R} + E_{\rm G}}{E_{\rm MR}}\right]\,, \tag{8.2a}$$

where E_{MR} is the magnetic rotator energy and E_R, E_G the base rotational and corrected gravitational energies, respectively,

$$E_{MR} = \Omega L\,, \qquad E_R = \frac{V_{\varphi,o}^2}{2} = \frac{\varpi_o^2\Omega^2}{2}\,,$$
$$E_G = \frac{V_{esc,o}^2}{2}\cdot\frac{\Delta\rho}{\rho_o} = \frac{\mathscr{GM}}{r_o}\left[1 - \frac{\rho_o(\text{pole})}{\rho_o(\alpha)}\right]\,. \tag{8.2b}$$

Thus, in a fast magnetic rotator (FMR) E_{MR} is larger than the sum of E_R, the rotational energy, and E_G, the gravitational energy corrected by the density latitudinal anisotropy factor $1-\rho_o(\text{pole})/\rho_o(\alpha)$, such that $\epsilon > 0$ in Eq. (8.2a) and the flow is asymptotically collimated by the magnetic rotator forces. Note that the ratio E_R/E_{MR} equals to the ratio of the cross section of the flow tube at the stellar surface to the cross section of the same tube at the Alfvén surface and therefore one expects that if this ratio is small compared to unity, the magnetic lever arm is much larger than the stellar base and thus angular momentum is efficiently extracted from the central object.

If on the other hand, the magnetic rotator energy E_{MR} is smaller than the sum of the rotational energy E_R and the corrected gravitational energy E_G such that $\epsilon < 0$ in Eq. (8.2a), the flow is asymptotically radial, as it is indeed the case for slow magnetic rotators (SMR). Note that the latitudinal anisotropy of the density ($\delta > 0$) favours radial asymptotics ($\epsilon < 0$) together with the rotational energy E_R. This result has been also obtained in the previous papers I and II where the solutions had a tendency to become more quickly radial as the effective gravitation is increased.

Consider the characteristic ratio $\epsilon/2\lambda^2$ at the asymptotic region of the outflow. *If* the flow obtains cylindrical asymptotics ($F = 2$), the available magnetic rotator energy is transfered into centrifugal kinetic and Poynting energy flux density per unit of mass flux density, such that at infinity,

$$\frac{\epsilon}{2\lambda^2} = \frac{V_{\varphi,\infty}^2/2 + S_\infty/\rho_\infty V_\infty}{L\Omega}\,. \tag{8.3a}$$

In this form it is evident that this quantity has to be positive in order to have collimation.

On the other hand, when rotation becomes negligible asymptotically, collimation is not possible and a sudden transition may appear towards a noncollimated asymptotical regime. In this case $G_\infty \longrightarrow \infty$, $M_\infty \longrightarrow \infty$ but $M_\infty^2/G_\infty^2 = V_\infty/V_\star$. Thus,

$$\frac{\epsilon}{2\lambda^2} = \frac{V_\infty M_\infty^2}{2\lambda^2 V_\star R^2}\left(\frac{F_\infty^2}{4} - 1\right) + \frac{V_\star}{V_\infty}\,, \tag{8.3b}$$

where $V_\star/V_\infty = G_\infty^2/M_\infty^2 \approx (G_\infty^2 - 1)/(M_\infty^2 - 1)$. Now since at infinity all forces vanish and the heating too disappears, the velocity should reach some constant value, V_∞. Then, if $0 < F_\infty < 2$ it follows from Eq. (3.8) that $G_\infty^2 = C^2R^{(2-F_\infty)}$ and $M_\infty^2 = V_\infty C^2 R^{(2-F_\infty)}$ where C is a constant. Inserting these expressions in Eq. (8.3b) it follows that negative values of $\epsilon/2\lambda^2$ are possible only for conical asymptotics where $F_\infty = 0$. Numerically it is also verified that the transition from positive to negative values of $\epsilon/2\lambda^2$ corresponds to a transition from cylindrical to conical asymptotics. Then, we reach the conclusion that if a central star is spinning down such that $\epsilon/2\lambda^2$ becomes negative, its outflow switches from one with cylindrical asymptotics (a jet) to one with a conical asymptotics (a wind), as we discuss in the following.

8.2. An example of non collimated outflow

Having illustrated in Sect. 7 collimated solutions, we present for the sake of completeness here an example of a non collimated solution. According to previous criterion we should seek such a solution when $\epsilon < 0$. In order to keep things as simple as possible, we took again $\delta\nu^2 = 2.96$ a value equal to the one obtained in model I [Figs. (7) and (8)]. We then lowered λ, which actually measures the strength of the magnetic rotator as explained in 8.1, to $\lambda = 1$. Again a unique solution, selected by an X-type point, is found to link the Alfvénic surface to the stellar surface. It corresponds to a negative value of ϵ such that no collimation to cylinders can occur. The parameters of model III are thus

$$\epsilon = -2.54\,,$$
$$\lambda = 1\,,$$
$$r_o = 3r_\odot\,. \tag{8.4}$$

Reducing the magnetic rotator strength, through λ^2, by about a factor of two, the jet has undergone a sudden transition from a purely collimated configuration with cylindrical shape towards an asymptotically radial shape reminding of the solar wind as shown in Fig. (11). A continuous transition through successive quasi-steady states described by our present modelling is not possible because it would go through a stage with $\epsilon = 0$. For $\epsilon = 0$, the jet would keep on accelerating and the temperature would keep on increasing up to infinity because the flow would never reach the third dynamical regime, as we have seen in Sect. 7.

However, through this example, we may understand that as a jet has removed enough angular momentum from a young star, the central object has span down making the magnetic rotator less efficient, reducing thus the magnetic rotator energy E_{MR}. After passing through a critical stage, cylindrical collimation and knot formation seems to have disappeared completely and the flow is undergoing a continuous expansion with magnetic pinching not efficient any longer.

From Fig. (8) to Fig. (11), the scenario has been oversimplified as compared to reality because we have kept $\delta\nu^2$ constant for simplicity. Globally, if the star reaches a stage comparable to the characteristics of the Sun today, it seems that $\delta\nu^2$ *at* the Alfvén surface may decrease which would shift the Alfvén surface to larger radii.

9. Summary

To obtain analytical solutions of the appropriate MHD equations for outflows from a central gravitating object (Sect. 2)

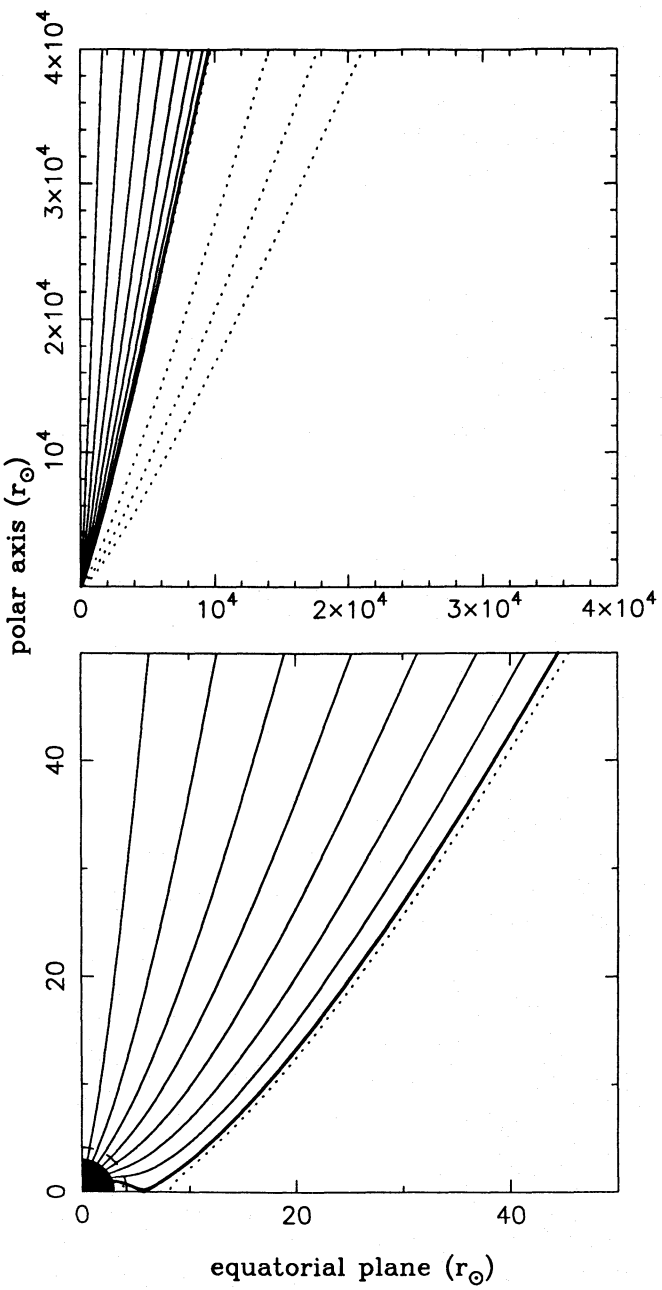

Fig. 11. Plot of the shape of the streamlines, as in Fig (8), for model III with $\epsilon = -2.54$, $\lambda = 1$. It corresponds to a star initially described by model I that spins down and reaches a non-collimated stage. The radial shape is made evident by the use of to different equatorial scale on the bottom and top part of the plot contrarily to previous figures. The solid lines are still lines connected to the star while dotted lines are connected to the disc

we have used streamline coordinates (R, α) and assumed that in these coordinates the key physical quantities of the problem are separable (Sect. 3). Further, expanding to lowest order their α-dependence,

$$M^2(R,\alpha) = \frac{\rho_a(\alpha)}{\rho(R,\alpha)} = M^2(R)\,, \qquad \frac{\varpi^2(R,\alpha)}{\varpi_a^2(\alpha)} = G^2(R)\,, \quad (9.1)$$

$$\rho_a(\alpha) = \rho_\star(1+\delta\alpha)\,, \qquad \varpi_a^2(\alpha) = r_\star^2\alpha\,, \quad (9.2)$$

$$\frac{d\dot{J}}{d\alpha} = \frac{\lambda}{4} r_\star^3 B_\star^3 \alpha\,, \qquad P(R,\alpha) = \frac{1}{2}\rho_\star V_\star^2 \Pi(R)(1+\kappa\alpha)\,, \quad (9.3)$$

we obtained a system of ordinary differential equations for $M(R)$, $G(R)$ and $\Pi(R)$ (Sect. 4). We have solved this system in the simpler case where $\kappa = 0$.

An integration of the coupled ODE's for $M(R)$, $G(R)$ and $\Pi(R)$ revealed that the asymptotic behavior of the streamlines of the flow crucially depends on the parameter $\epsilon/2\lambda^2$ which is a measure of the available magnetic rotator energy such that, in a FMR, $\epsilon/2\lambda^2 > 0$ and the streamlines obtain cylindrical asymptotics while, in a SMR, $\epsilon/2\lambda^2 < 0$ and the streamlines become asymptotically conical (Sect. 5). Note, in passing, that FMR and SMR do not relate to the actual speed of rotation; a T-Tauri jet is a FMR although the star itself does not spin very fast. In addition, in the case of the FMR, collimation is achieved through oscillations in the form of the streamlines. We derived an analytical expression for the wavelength of these oscillations by expanding the momentum equation in the asymptotic regime. We have shown that these oscillations can arise from the interplay of toroidal components only, without the help of pressure gradients. This result is novel with respect to previous studies showing such oscillations.

A detailed study of the solutions (Sect. 6) showed that three categories of topologies exist depending on the rotational speed of the central star. Nevertheless, the topologies of the solutions are controlled by an X-type critical point in the subAlfvénic regime (Sect. 6) in addition to the classical Alfvénic transition (Sect. 4); and this result generalizes to a rotating object the study of Paper II for non rotating flows. Although rough estimates linking the boundary conditions at the source of the outflow to the transAlfvénic region may be obtained (Sect. 7), a consistent solution of the equations of the outflow from the wind source to infinity crossing the relevant critical surfaces is needed; this problem is not a trivial one and should be taken into account in related numerical studies.

A preliminary application of the results to outflows from young stellar objects (YSO's) has been performed (Sect. 7) suggesting a simple way to use observations to constrain the model. We emphasized that there is a necessity for a two component jet constituted of an inner core of stellar origin surrounded by a wind coming from the disc. The disc wind may be a good candidate to explain most of the observed features. However the stellar jet may still be an essential ingredient for solving consistently the problem, carrying the necessary poloidal current that supports the collimated flow. More precisely, the present model is appropriate to describe some basic features of optical jets as they come from both the star and the inner disc region. On the other hand, the mass loss associated with CO lobes could be originating in the extended disc region which has not been at the main focus of our modelling. Of course models which are stationary like the present one cannot account for the observed proper motions in HH objects. However stationary models can be used as the first step for an understanding of the time dependent evolution of outflows from YSOs. In this connection,

proper motions can be undestood as resulting from a variability of the source region of the outflow (Raga et al. 1993).

We finally concluded (Sect. 8) by giving a criterion for collimation of the flow in terms of quantities at its source. We suggested that the asymptotic shape of the streamlines of a rotating object must drastically change as it losses angular momentum and successively passes from the stage of a rapidly rotating YSO (FMR) to a stage of a solar-like object (SMR).

We would like to emphasize two limits of the present model as we have already discussed throughout the paper together with some possible solutions.

In the present study we confined ourselves for simplicity to a spherically symmetric pressure, i.e., the case $\kappa = 0$. However, the same model can be easily extended to include a meridionally anisotropic pressure ($\kappa \neq 0$). Such a general pressure gradient may play an important role in the initial part of the acceleration. Thus, if $\kappa < 0$ an external pressure confinement may help the collimation, although there is no such observational evidence that the jet should be pressure confined. Conversely, with $\kappa > 0$ it would be possible to increase the value of δ keeping $(\delta - \kappa)$ fixed to the previous value of δ used in model I. In such a case the gravitational effect which is proportional to $(\delta - \kappa)\nu^2$ would remain the same while the meridional anisotropy in the density would increase more rapidly. In particular for collimated solutions, the inner core of our hollow jet would be more confined around the axis. The anisotropy in the pressure would also allow to have a reduced pressure along the axis, which we have seen to be a way to reduce the high asymptotic temperature obtained along the polar axis. Moreover, increasing δ would increase the total mass loss rate and this would allow to reduce the size of the source of the observed mass loss rates to an even smaller inner region of the disc wind. Although we have just shown that such a study may easily improve the connection with observations, we do not expect to find completely new fundamental results. For example, concerning the asymptotic oscillations, a more general model including tranverse pressure gradients is likely to reproduce intermediate results between those presented here and previous other studies e.g., Chan & Henriksen (1980). Nevertheless for the sake of completeness and a better understanding of the inner accelerating region, such a study has to be undertaken.

Another question which has not been fully addressed here, relates to the disc wind. We have shown that a current density singularity at the jet axis can be avoided and collimation still achieved in a natural way without a complete focusing toward the axis, contrary to cold plasma models, by a simple expansion scheme of the MHD free functions. And although the present model does not use the most general form of those free functions, it remains of a quite general nature around the axis since it includes the dominant terms that exist there. However, another form of these free functions may be more appropriate to describe the outer part of the jet. For example, we have already noted that our model would need somehow an outer cut off, or to be replaced by a current free solution at large distances from the jet-axis. Since our main goal has been here to find a criterion distinguishing collimated stellar jets from non collimated solar-type stellar winds, it was beyond our scope to describe in detail the interesting physical problem posed by a disc wind.

Nevertheless it is interesting to compare the asymptotic regimes obtained to the litterature. We have shown that the flow can reach cylindrical or radial asymptotics. In the case of radial asymptotics the flow is asymptotically isothermal as in Tsinganos & Trussoni (1992), so there is no contradiction with the result of Heyvaerts & Norman (1989) where only non-isothermal flows have been considered. Moreover it is likely in this case, as the terminal temperature is rather low, that the flow is no longer ionized. We suggest then that the flow would become a radial hydrodynamical adiabatic flow far from the star. From non collimation to full collimation, we have found only one paraboloidal solution with infinite terminal velocity carrying no poloidal current in agreement with Heyvaerts & Norman (1989). The last interesting regime is composed of collimated solutions which reach cylindrical asymptotics and carry a net poloidal current. Again this is in agreement with the conclusions of Heyvaerts & Norman (1989).

In Sakurai's treatment a *paraboloidal* (almost cylindrical) structure with a logarithmically increasing cylindrical radius is obtained (despite the deceiving logarithmic plot of the streamlines where they seem to converge towards the pole). Apparently the jet is not completely collimated along the axis. However, it generates a high density column along the axis which is likely to be unstable according to the author. Conversely to this model we have been able to obtain fully collimated stationary solutions with a hollow jet structure.

Note that contrarily to Blandford & Payne's (1982) and Pelletier & Pudritz's (1992) models we do not find streamlines that keep on converging towards the axis, which is choking off the solution after some radius unless shocks are invoked (see Gomez de Castro & Pudritz 1993). However the analytical expressions given by Blandford & Payne (1982) for the asymptotics quantities (e.g. their Eqs. 2.32 - 2.35) should not be valid near the axis as they have neglected centrifugal forces. Moreover, from the expressions of the toroidal components, we see that the jet radius in the superAlfvénic regime should never be less than the Alfvén radius (Pelletier & Pudritz 1992). Note also that an inner source for the net poloidal current has to be invoked in Pelletier & Pudritz's model that could be of the kind described here. Nevertheless a common feature of all these models is the first recollimation process that occur for sufficiently high terminal velocities and Alfvén numbers.

Contrarily to cold plasma models, the decollimation / recollimation process is probably due to the self consistent treatment of the current along the axis and the role of the centrifugal forces. This is quite different from the Chan & Henriksen (1980) result where an internal pressure was always important there to support the pinching force. As we already mention, this basic difference is also responsible for the different nature of our oscillations as compared to theirs and the existence of a damping length in our case which does not exist there (see Appendix B in Chan & Henriksen (1980) where the authors wrote an equation for the oscillations similar to ours but droping the centrifugal term and keeping the internal pressure gradient). The advantage we get

in our formulation is a broader range of wavelengths that may explain oscillations on smaller scales of the jets.

To conclude with, the scope of this paper has been to give a criterion for the collimation of an outflow. As we have shown, this can be interpreted in terms of the meridional anisotropy of the volumetric generalized Bernoulli energy at the source of the outflow. A cylindrically collimated jet requires an excess in this Bernoulli energy at any nonpolar streamline, in comparison to a polar streamline.

Acknowledgements. We are indebted to Dr Edo Trussoni for stimulating discussions during the course of this work and Dr A.C. Raga for reading and commenting the manuscript. We acknowledge a bilateral scientific agreement between France and Greece that made possible our respective visits to Heraklion and Paris.

References

Begelman M.C., Li Z-Y., 1994, ApJ (in press)
Belcher J.W., MacGregor K.B., 1976, ApJ, 210, 498
Bertoux C., Basri G., 1991, Properties and Models of T Tauri Stars. In: Lada C.J., Kylafis N.D. (eds.) Proc. NATO ASI The Physics of Star Formation and Early Stellar Evolution. Kluwer, Dordrecht, p. 649
Bouvier J., Bertout C., Benz W., Mayor M., 1986, A&A, 165, 110
Blandford R.D., Payne D.G., 1982, MNRAS, 199, 883
Gomez de Castro A.I., Pudritz R.E., 1993, ApJ, 409, 748
Cassinelli J.P., 1990. In: Willson L.A., Stalio R. (eds.) Angular Momentum and Mass Loss for Hot Stars. Kluwer, Dordrecht, p. 135
Chan K.L., Henriksen R.H., 1980, ApJ, 241, 534
Contopoulos J., Lovelace R.V.E., 1993. In: Dermott S., Hunter J.H., Wilson R. (eds.) Proc. of Seventh Florida Workshop: Astrophysical Disks, New York Academy of Sciences, New York, p. 295
Heinemann M., Olbert S., 1978, J. of Geophys. Res., 83-A6, 2457
Heyvaerts J., Norman C.A., 1989, ApJ, 347, 1055
Hughes P.H., 1991, Beams and Jets in Astrophysics. Cambridge Astrophysics Series, Cambridge University Press, Cambridge
Koupelis T., Van Horn H.M., 1989, ApJ, 342, 146
Koupelis T., 1990, ApJ, 363, 79
Lada C.J., 1985, ARA & A, 23, 267
Li Z-Y., 1993, ApJ, 415, 118
Lima J.J., Priest E., 1993, A&A, 268, 641
Lovelace R.V.E., Berk H.L., Contopoulos J., 1991, ApJ, 379, 696
Low B.C., Tsinganos K., 1986, ApJ, 302, 163
Marcheto F., 1992. In: Roland J., Sol H., Pelletier G. (eds.) From Beams to Jets, Cambridge University Press, Cambridge, p. 309
Malbet, F. 1993, Environnement Circumstellaire des Etoiles Jeunes, thèse de doctorat. Université Paris VII, Paris
Mestel L., 1968, MNRAS, 138, 359
Mestel L., Spruit H.C., 1987, MNRAS, 226, 57
Mundt R., 1986. In: Black D., Matthews M., (eds.) Protostars and Planets II. Univ. Arizona Press, Tucson, p. 414
Munro R.H., Jackson B.V., 1977, ApJ, 213, 874
Natta A., Giovanardi C., 1991, The Physics of Neutral Winds from Low Mass Young Stellar Objects. In: Lada C.J., Kylafis N.D. (eds.) Proc. NATO ASI The Physics of Star Formation and Early Stellar Evolution. Kluwer, Dordrecht, p. 595
Nerney S.F., Suess S.T., 1975a, ApJ, 196, 837
Nerney S.F., Suess S.T., 1975b, ApJ, 200, 503
Nerney S.F., Suess S.T., 1975c, Solar Phys., 45, 255
Nerney S.F., Suess S.T., 1985, ApJ, 296, 259
Norman C.A., Pudritz R.E., 1986, ApJ, 301, 571
Owen F.N., Hardee P.E., Cornwell T.J., 1989,ApJ , 340, 698
Parker E.N., 1963, Interplanetary Dynamical Processes. Interscience, New York.
Pelletier G., Pudritz R.E., 1992, ApJ, 394, 117
Pudritz R.E., Norman C.A., 1983, ApJ, 274, 677
Raga A.C., Cantó G., Biro S., 1993, MNRAS, 260, 163
Rees M.J., 1971, Nat, 229, 312-510
Reipurth B., 1991, Herbig-Haro Objects. In: Lada C.J., Kylafis N.D. (eds.) Proc. NATO ASI The Physics of Star Formation and Early Stellar Evolution. Kluwer, Dordrecht, p. 497
Sakurai T., 1985, A&A, 152, 121
Sakurai T., 1987, PASJ, 39, 821
Sakurai T., 1990, Computer Physics Reports, 12, 247
Schatzman E., 1962, Ann. Astrophys., 25, 1
Shibata K., Uchida Y., 1986, PASJ, 38, 631
Shibata K., Uchida Y., 1987, PASJ, 39, 559
Trussoni E., Tsinganos K., 1993, A&A, 269, 589
Tsinganos K., 1982, ApJ, 252, 775
Tsinganos K., Low B.C., 1989, ApJ, 342, 1028
Tsinganos K., Sauty C., 1992a, A&A, 255, 405 (Paper I)
Tsinganos K., Sauty C., 1992b, A&A, 257, 790 (Paper II)
Tsinganos K., Trussoni E., 1990, A&A, 231, 270
Tsinganos K., Trussoni E., 1991, A&A, 249, 156
Tsinganos K., Surlantzis G., Priest, E. 1993, A&A (in press)
Tsinganos K., Trussoni E., Sauty, C. 1993, Outflow Focusing in Rotating Stellar Magnetospheres. In: Linsky J., Serio S. (eds.) Advances in Stellar and Solar Coronal Physics. Kluwer, Dordrecht (in press)
Tsinganos K., Vlastou G., 1988, A&A, 193, 125
Weber E.J., Davis L., 1967, ApJ, 148, 217

This article was processed by the author using Springer-Verlag TEX A&A macro package 1992.